

Choosing the Threshold in Extreme Value Analysis

Léo R. Belzile^{1,a}  and Anthony C. Davison^{2,b} 

¹*Department of Decision Sciences
HEC Montréal
3000, chemin de la Côte-Sainte-Catherine
Montréal (Québec)
Canada, H3T 2A7
^aleo.belzile@hec.ca*

²*Institute of Mathematics
École polytechnique fédérale de Lausanne
EPFL-SB-PH, Station 8
1015 Lausanne
Switzerland
^banthony.davison@epfl.ch*

Abstract. One of the two dominant approaches for univariate extreme value analysis is to model exceedances above a large threshold, the choice of which has a large impact on inference and whose uncertainty is often subsequently ignored. In this article we review more than 40 threshold selection procedures, including semiparametric methods based on Hill’s estimator, visual diagnostics, goodness-of-fit tests, and others based on extended generalized Pareto models. Starting with the statistical properties underlying the various proposals, we provide a critical assessment of their strengths and weaknesses, discuss how they might be automated and describe the results of an extensive simulation study used to identify the most promising procedures. The approaches are compared using a long time series of daily rainfall totals from Padova.

1 Introduction

Natural catastrophes and economic disasters have impacted much of the globe over the past two decades, leading to a widespread appreciation of the potential impacts of rare events. A central role in the study of such events is played by extreme-value analysis, which employs statistical models to extrapolate from the data available to more severe, as-yet unseen, risks. The visibility of this domain of statistics has greatly increased, with a large community of researchers working on all of its aspects and mounting application of related methods.

Extreme-value theory is usually developed in terms of large events, typically analysed either as maxima of blocks of successive observations, or as exceedances above some high threshold. These approaches are linked by a unifying asymptotic framework that combines the theories of point processes for event times and of regular variation for event sizes. These limiting results provide asymptotic models that are fitted to non-asymptotic data, so an adequate fit of the models to the data is crucial to subsequent inferences, and in particular determines the trustworthiness of any extrapolation.

The initial theoretical results and applications of extreme-value theory considered block maxima (Fisher and Tippett, 1928; Gnedenko, 1943; Gumbel, 1958), but in the early 1970s attention turned to threshold exceedances (Todorovic and Zelenhasic, 1970; Todorovic and Rousselle, 1971; Balkema and de Haan, 1974; Pickands, 1975), and since the introduction of related statistical methods (Davison, 1984; Smith, 1984; Davison and Smith, 1990), the so-called ‘peaks over threshold’ (POT) approach has become widely applied. The key idea is

Keywords and phrases. generalized Pareto distribution, Padova rainfall series, peaks over threshold analysis, penultimate approximation, statistics of extremes, threshold selection.

that the extremes of data from a stationary time series be modelled by considering only those observations Y that exceed a threshold u , since under mild conditions it can be shown that there exists a positive function σ_u such that as u approaches the upper support point of Y ,

$$\Pr\{(Y - u)/\sigma_u > x \mid Y > u\} \rightarrow (1 + \xi x)_+^{-1/\xi}, \quad x > 0, \quad (1)$$

uniformly in x . Here $b_+ = \max(b, 0)$ and the parameter ξ takes values in the real numbers; the right-hand side of eq. (1) is replaced by $\exp(-x)$ when $\xi = 0$. This implies that an exceedance $X = Y - u$ over a sufficiently high threshold u approximately follows the generalized Pareto distribution (GPD), i.e.,

$$\Pr(X \leq x) \approx G(x) = \begin{cases} 1 - (1 + \xi x/\sigma_u)_+^{-1/\xi}, & \xi \neq 0, \\ 1 - \exp(-x/\sigma_u), & \xi = 0, \end{cases} \quad x > 0. \quad (2)$$

Below we write $X \sim \text{GP}(\sigma_u, \xi)$ when X has the distribution on the right-hand side of eq. (2), and use Y to denote general random variables.

The distribution (2) depends on two parameters. The shape parameter ξ determines the upper tail weight of the density function, which is Pareto-like when $\xi > 0$, exponential for $\xi = 0$, and has support only in the interval $(0, -\sigma_u/\xi)$ when $\xi < 0$. We shall see below that the scale parameter σ_u depends on the chosen threshold u .

In the simplest applications a high but finite threshold u is chosen using the available data, the parameters of eq. (2) are estimated from the n_u exceedances over u , and this fitted model is used for extrapolation, often to values of x that lie beyond the observed sample. The $(1 - 1/T)$ -quantile of the distribution of annual maxima, or T -year return level ($T > 1$), is often the target of inference. In practice there may be numerous complications, most commonly that the series is non-stationary and that local dependence leads to the clustering of exceedances. In the original applied literature only the largest observation (the ‘peak’) in each cluster was retained, but in line with current usage we shall use the abbreviation POT to refer to this entire approach to extremes.

There is a further trade-off between quality of fit to the available data and extrapolation beyond them. In Section 2.1, we shall see that expression (2) is rather flexible, and that “penultimate” approximations to the left-hand side of eq. (1) have the same form with different parameter values. This implies that a good fit to the available data should be balanced against the quality of extrapolation to higher, especially much higher, quantiles. It also suggests that different approaches to choosing the threshold u may be appropriate when the purpose of an analysis is to estimate a particular parameter, such as a value-at-risk or an expectile, rather than to fit a model for subsequent general use.

The choice of threshold u is critical to the successful application of POT methods, and the goal of this paper is to review methods of choosing it. Taking u too high means that the number of exceedances n_u is small, thus increasing the uncertainty of subsequent inferences, whereas taking u too low may lead to poor extrapolation owing to the inclusion of non-extreme data. This trade-off has led to many suggestions for threshold selection, ranging from simple graphical procedures using stability properties of the GPD (e.g., Davison and Smith, 1990; Coles, 2001) to sophisticated analytical procedures requiring stringent restrictions on the tail of Y . Certain procedures were compared numerically in Gomes and Oliveira (2001), Schneider, Krajina and Krivobokova (2021), Murphy, Tawn and Varty (2025) and elsewhere. The most comprehensive previous reviews of threshold selection are Scarrott and MacDonald (2012), Caeiro and Gomes (2016) and Langousis et al. (2016). Scarrott and MacDonald (2012) cover the main ideas, with a focus on the splicing models described in Section 4.3. Most of the methods covered by Caeiro and Gomes (2016) are semiparametric (cf. Section 6). Many further procedures for threshold selection have been proposed since these articles and book chapter appeared and are reviewed for the first time here.

We illustrate our discussion using daily rainfall data from Padova (Marani and Zanetti, 2015). Exploratory analysis reveals strong seasonality, particularly for the number of rainy days, which form around 25% of the total; we reduce the effect of such artefacts by taking only the months of July–September for the years 1878–2016, yielding $n = 3311$ rainfall totals over 2mm. Although there are fewer rainy days during these summer months, the corresponding episodes of precipitation can be more extreme. For simplicity and since our objective is to illustrate and compare the results of threshold selection procedures, we treat the summer data as stationary.

The paper is organized as follows. In Section 2, we sketch properties of the generalized Pareto distribution, and then in the following three sections describe threshold selection procedures. These can be broadly categorized based on the approach taken: threshold stability (Section 3), extension of the GPD (Section 4), goodness-of-fit methods (Section 5), or semi-parametric procedures when $\xi > 0$ (Section 6). Section 7 outlines the results of extensive comparisons fully described in Appendices C and D and the results of applying the selection methods to the Padova series; other appendices give details for which there is insufficient space in the paper. Section 8 contains a brief general discussion.

2 Generalized Pareto distribution

2.1 Basic notions

2.1.1 First- and second-order conditions The generalized Pareto limit of (1) for rescaled threshold exceedances hold in wide generality. Let Y be a random variable with distribution function F , define $F^-(p) = \inf\{y : F(y) \geq p\}$ for $p \in (0, 1)$, and for $t > 1$ let $b(t) = F^-(1 - 1/t)$. Then the so-called first order condition, which yields the generalized Pareto limit, holds if there exists a positive function a such that (de Haan and Ferreira, 2006, Theorem 1.1.6)

$$\lim_{t \rightarrow \infty} \frac{b(ty) - b(t)}{a(t)} = \int_1^y s^{\xi-1} ds = \begin{cases} (y^\xi - 1)/\xi, & \xi \neq 0, \\ \log y, & \xi = 0, \end{cases} \quad y > 0.$$

A simple interpretation of the roles of $a(\cdot)$ and ξ is possible if F is twice differentiable and has cumulative hazard function $\mathcal{H}(y) = -\log\{1 - F(y)\}$ and reciprocal hazard function $r(y) = 1/\{d\mathcal{H}(y)/dy\}$. Then we can take $a(t) = r\{b(t)\}$, write $\xi_t = r'\{b(t)\}$, and find that $\xi = \lim_{t \rightarrow \infty} \xi_t$.

Smith (1987) shows that taking (2) with ξ_t rather than ξ may give a better, so-called penultimate, approximation to the left-hand side of (1). A well-known case is the limiting exponential distribution for Gaussian exceedances, for which $\xi = 0$, which is reached so slowly that for all practical purposes the shape parameter is negative (Fisher and Tippett, 1928), and this is what is found when fitting (2) to Gaussian data. Such slow convergence might seem worrisome, but in practice the major issue is whether the GPD can provide useful extrapolations from data to levels likely to be used in applications, and of course this depends on the context. We illustrate this numerically in Section B.

Penultimate approximations can be related to further tail properties of F , which is said to be generalized regularly varying of second order at infinity if there exists a function $A(t)$ such that (de Haan and Ferreira, 2006, §2.3)

$$H_{\xi, \rho}(y) := \lim_{t \rightarrow \infty} \frac{b(ty) - b(t) - a(t) \int_1^y s^{\xi-1} ds}{a(t)A(t)} \quad (3)$$

$$= \int_1^y s^{\xi-1} \int_1^s u^{\rho-1} du ds, \quad y > 0, \rho \leq 0, \quad (4)$$

and such that $H_{\xi,\rho}(y)$ is not proportional to $\int_1^y s^{-\xi-1} ds$. The second-order auxiliary function $A(t)$ is regularly varying at infinity with tail index $\rho \leq 0$, i.e., $\lim_{t \rightarrow \infty} |A(ty)/A(t)| = y^\rho$ for $\rho \leq 0$, and also $\lim_{t \rightarrow \infty} A(t) = 0$ with $A(t)$ ultimately not changing sign, so $\text{sign}\{A(y_s)\} = \text{sign}\{A(t + y_s)\}$ for some $y_s > 0$ and for all $t > 0$. If $b(t)$ is twice differentiable and $b'(t)$ is eventually positive, then (de Haan and Resnick, 1996, Theorem 2.1)

$$A(t) := \frac{tb''(t)}{b'(t)} - \xi + 1 = r'\{b(t)\} - \xi = \xi_t - \xi; \quad (5)$$

this is the difference between the penultimate and limiting values of the shape parameter. Bücher and Zhou (2021) discuss these and similar conditions that apply to block maxima.

Many methods mentioned in Section 6 focus on the Hall and Welsh (1985) class of distributions, whose survival function admits the asymptotic expansion

$$1 - F(y) = \alpha y^{-1/\xi} \left\{ 1 + \beta y^{\rho/\xi} + o(y^{\rho/\xi}) \right\}, \quad y \rightarrow \infty, \quad (6)$$

equivalent to a polynomial second-order auxiliary function $A(t) = \beta t^\rho$ for $\beta \neq 0$ and $\rho < 0$.

Although useful in theoretical work, the second-order functions such as A or $H_{\xi,\rho}$ turn out to be extremely difficult to estimate, and it seems impossible to exploit this further structure in data analysis.

2.1.2 Threshold stability The GPD is threshold-stable: if $Y - u \sim \text{GP}(\sigma_u, \xi)$ and $v > u$ is such that $\Pr(Y > v) > 0$, then the conditional distribution of $Y - v$ given $Y > v$ is also GPD, with the same ξ and scale parameter $\sigma_v = \sigma_u + \xi(v - u)$. When $\xi < 1$ we have $\text{E}(Y - u) = \sigma_u/(1 - \xi)$, so $\text{E}(Y - v | Y > v) = \{\sigma_u + \xi(v - u)\}/(1 - \xi)$. This is the basis for threshold stability plots, which display the empirical version of this conditional expectation and should be linear in v if the GPD is adequate. The property also suggests diagnostics obtained by fitting the model over a grid of thresholds.

2.1.3 Inhomogeneous Poisson process formulation The GPD can also be derived from a limiting Poisson process \mathcal{P} under which events occur in the (t, y) -plane with measure

$$\Lambda[(t', t) \times [u, \infty)] = (t - t') \left\{ 1 + \xi(u - \eta)/\tau \right\}_+^{-1/\xi}, \quad u \in \mathbb{R}, t > t', \quad \eta \in \mathbb{R}, \tau > 0.$$

The measure of the set $\mathcal{C}_u = [0, 1] \times [u, \infty)$ under this model is

$$\mu(u) = \left\{ 1 + \xi(u - \eta)/\tau \right\}_+^{-1/\xi}, \quad (7)$$

so the probability that the restriction of \mathcal{P} to \mathcal{C}_u has no points in \mathcal{C}_{u+x} for $x > 0$ is $\mu(x + u)/\mu(u) = (1 + \xi x/\sigma_u)_+^{-1/\xi}$, where $\sigma_u = \tau + \xi(u - \eta)$, corresponding to eq. (1). The vertical coordinates of the Poisson process \mathcal{P} on $\mathcal{C}_{-\infty}$ can be generated by transforming a unit-rate Poisson process on the positive half line, $E_1, E_1 + E_2, \dots$, where the E_j are independent standard exponential random variables, into the inhomogeneous process with points

$$\eta + \frac{\tau}{\xi} \left\{ \left(\sum_{j=1}^r E_j \right)^{-\xi} - 1 \right\}, \quad r = 1, 2, \dots, \quad (8)$$

which lie in the subset of the real line for which $\mu(x) > 0$. Hence if we use an estimate of μ to transform the data to a unit-rate Poisson process, the choice of threshold amounts to choosing the smallest value of u above which the transformed observations are consistent with this process.

2.1.4 *Martingale residuals* The Markov properties of the order statistics $X_{(1)} \leq \dots \leq X_{(n)}$ of a $\text{GP}(\sigma, \xi)$ random sample, which follow from the Poisson process construction described in Section 2.1.3, allied to threshold stability, imply that the joint density of the order statistics can be written as

$$\prod_{j=2}^n f(x_{(j)} | x_{(j-1)}) f(x_{(1)}) = \prod_{j=1}^n \frac{1}{\sigma_j} \left\{ 1 + \frac{\xi}{n+1-j} \frac{(x_{(j)} - x_{(j-1)})}{\sigma_j} \right\}_+^{-(n+1-j)/\xi-1}, \quad (9)$$

where $\sigma_j = (\sigma + \xi x_{(j-1)}) / (n+1-j)$ and $x_{(0)} = 0$ (cf. Oorschot, Segers and Zhou, 2023, Appendix A). This extends the Rényi (1953) representation for exponential data, as the smallest order statistic $X_{(1)} \sim \text{GP}(\sigma/n, \xi/n)$ and the increments $X_{(j)} - X_{(j-1)}$, conditional on $X_{(j-1)} = x_{(j-1)}$ have $\text{GP}\{\sigma_j, \xi/(n+1-j)\}$ distributions, for $j = 2, \dots, n$, in addition to being conditionally independent of the lower order statistics. Stein (2023) explores using this representation to replace choosing the threshold by weighting the observations.

2.2 Statistical properties of the generalized Pareto distribution

In this paper we consider the choice of threshold u , either within a fixed grid of ordered thresholds $u_1 < \dots < u_J$ or within a subset of the order statistics $Y_{(1)} < \dots < Y_{(n)}$ of a random sample Y_1, \dots, Y_n ; we write \mathcal{U} for the grid and call it fixed or random, respectively.

If u is chosen, then we fit (2) using the n_u positive values of $Y_j - u$; n_u is then random. Conversely we may choose n_u and take $u = Y_{(n-n_u)}$ as the (random) threshold. As the limit in (1) holds as u increases to the upper support point y_+ of Y , we must use a so-called intermediate sequence for which $n_u/n \rightarrow 0$ as $n \rightarrow \infty$ in order for the estimator to be consistent, so that as n_u increases the number of exceedances retained grows but comprises an increasingly small proportion of the original data. Simple rules such as using a fixed proportion of the data by setting $n_u \approx np$ for some fixed p are inappropriate; we must rather use smaller fractions n_u/n in larger samples, for example taking the $\lceil n - n^q \rceil$ largest order statistics, with $q = 0.995$ or $q = 0.999$. In practice a minimum number of observations is needed for fitting, whatever the size of the entire sample, so we must have $n_u \geq 20$, say.

2.2.1 *Maximum likelihood estimator* Maximum likelihood estimation makes no assumption on the sign of the shape parameter and is readily extended to more complex settings; the parameter estimators have large-sample normal distributions if eq. (1) holds and $\xi > -1/2$ (Smith, 1985), though the normal approximation may be poor in small samples (Süveges and Davison, 2010). Numerical problems can arise when $\xi < 0$, because the support of the density, $\{x : \sigma_u + \xi x > 0\}$, then depends on the parameters, but these can be eased using a reparametrisation due to R. L. Smith (cf. Davison, 1984) that reduces the optimization to a unidimensional problem (Grimshaw, 1993) by expressing the model in terms of ξ and $\eta = -\xi/\sigma_u$. Apart from constants and when $\eta \neq 0$, its profile log likelihood,

$$\ell_p(\eta) = -n \log \left\{ -\frac{1}{n\eta} \sum_{i=1}^n \log(1 - \eta x_i) \right\} - \sum_{i=1}^n \log(1 - \eta x_i), \quad \eta < 1/x_{(n)},$$

attains an overall maximum of $+\infty$ as $\eta \rightarrow 1/x_{(n)}$ and has a global maximum if the sample coefficient of variation exceeds unity and $\xi > 0$ (del Castillo and Daoudi, 2009).

The asymptotic covariance matrix of the maximum likelihood estimators $(\hat{\sigma}_u, \hat{\xi})$ depends on whether u is fixed or an order statistic (Drees, Ferreira and de Haan, 2004, Remark 2.3), though $\hat{\xi}$ has asymptotic variance $(1 + \xi)^2$ in both cases (Drees, Ferreira and de Haan, 2004, Corollary 2.1). These estimators can have large bias in small samples.

2.2.2 Hill's estimator The well-known [Hill \(1975\)](#) estimator of a positive shape parameter ξ averages the log spacings of the n_u largest order statistics of a random sample relative to the random threshold $u = Y_{(n-n_u)}$, assumed to be positive:

$$H_{n,n_u} = \frac{1}{n_u} \sum_{i=1}^{n_u} \{\log Y_{(n-i+1)} - \log Y_{(n-n_u)}\}. \quad (10)$$

If the upper tail is Pareto-like ($\xi > 0$), the [Weissman \(1978\)](#) estimator of the quantile at level $1 - p$ is $Q_{n_u}(1 - p) = Y_{(n-n_u)} \{n_u/(pn)\}^{H_{n,n_u}}$. Although H_{n,n_u} is consistent for $\xi > 0$ for an intermediate sequence n_u , it is not location-invariant. Less widely-used estimators for real-valued ξ include the moment estimator of [Dekkers and de Haan \(1989\)](#), those based on generalized median, trimmed mean and mean excess functionals of [Beirlant, Vynckier and Teugels \(1996a\)](#), and a location-scale invariant estimator based on an extreme U -statistic ([Oorschot, Segers and Zhou, 2023](#)); the last uses log spacings and thus is undefined in the presence of ties. For the latter, as well as for the shape estimator of [Wager \(2014\)](#), more work is needed to derive accompanying estimators of scale and quantiles, along with confidence intervals.

A sufficient condition for asymptotic normality of Hill's estimator is second order regular variation (cf. Section 2.1.1) with $\lim_{n_u \rightarrow \infty} n_u^{1/2} A(n/n_u) = \lambda \in \mathbb{R}$, subject to which ([de Haan and Ferreira, 2006](#), Theorem 3.2.5)

$$n_u^{1/2}(H_{n,n_u} - \xi) \rightarrow \text{normal}\{\lambda/(1 - \rho), \xi^2\}, \quad \rho \leq 0. \quad (11)$$

The asymptotic bias of $\lambda/(1 - \rho)$, which is unknown in applications, is thus dictated by the rate at which the number of extreme observations grows relative to the total sample size and by the function $A(t)$, which is distribution-specific. Hill's estimator has a smaller asymptotic variance than the maximum likelihood estimator, but is restricted to positive values of ξ .

2.2.3 L -moments Probability weighted moments are often used for estimation in hydrological applications. For a generalized Pareto variable X with $\xi < 1$ we can define $\alpha_r = E[X\{1 - F(X)\}^r] = \sigma/\{(1+r)(1+r-\xi)\}$ ($r = 0, 1, \dots$), yielding estimators based on the identities $\xi = -\alpha_0/(\alpha_0 - 2\alpha_1) + 2$ and $\sigma = 2\alpha_0\alpha_1/(\alpha_0 - 2\alpha_1)$ with the α_r replaced by empirical counterparts ([Hosking and Wallis, 1987](#), eq. 5). Such estimators are linear in the observations, and thus have good small-sample properties. They are closely related to L -moments ([Hosking, 1990](#)), which are linear combinations of probability weighted moments of the form

$$\lambda_s = \sum_{r=0}^{s-1} (-1)^{s-1-r} \binom{s-1}{r} \binom{s-1+r}{r} \alpha_r, \quad s = 1, 2, \dots$$

Another estimator based on the L -skew, $\tau_3 = \lambda_3/\lambda_2$, takes $\xi_{\text{lmom}} = (3\tau_3 - 1)/(1 + \tau_3)$ and $\sigma_{\text{lmom}}(1 - \xi_{\text{lmom}})(2 - \xi_{\text{lmom}})\lambda_2$, where $(\sigma_{\text{lmom}}, \xi_{\text{lmom}})$ are obtained by replacing probability weighted moments by their unbiased estimators.

2.2.4 Padova data Figure 1 illustrates the variability of shape estimates obtained using different estimators applied to the Padova data. The U -statistic-based estimator of [Oorschot, Segers and Zhou \(2023\)](#) varies smoothly, but the others are sensitive to the threshold. Estimators from nearby thresholds are strongly correlated. The Hill estimator yields very large return levels as n_u increases, due to the extrapolation with large shape values. The maximum likelihood and L -moment estimator (not shown) are rather stable and near identical, both close to the results of a Bayesian analysis.

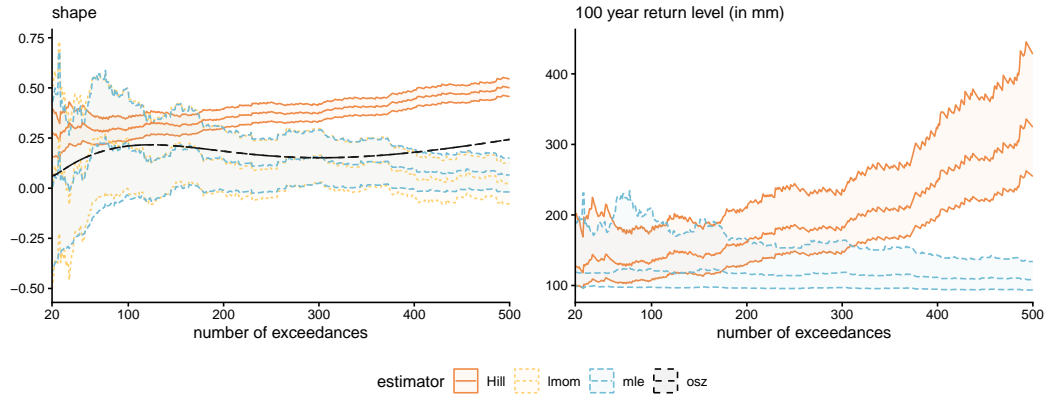


Figure 1 Variation with the threshold of shape parameter estimates (left) and 100-year return levels (right) for different estimators: the maximum likelihood and (MLE) L-moments (lmom) (Hosking and Wallis, 1987) of the generalized Pareto parameters, the Hill (1975) estimator, and the U-statistic estimator of Oorschot, Segers and Zhou (2023) (osz). Shape estimates are shown with Wald-based 95% confidence intervals. The MLE and L-moments return levels are based on the GPD quantile function and with 95% profile-likelihood confidence intervals, ignoring variation due to the random number of exceedances, whereas the Hill estimator uses the Weissman (1978) quantile estimator with the saddlepoint confidence interval estimator of Buitendag, Beirlant and de Wet (2020).

In most applications good estimation of σ_u and ξ is not the goal of analysis, and a key aspect is stability of extrapolation to risk functionals such as high quantiles. Figure 1 shows that, while the maximum likelihood estimates of the shape parameter are rather variable, the quantile estimates are more or less constant, whereas those based on the Weissman estimator increase steadily as the number n_u of exceedances grows.

3 Methods based on stability

3.1 Moment stability plots

Threshold stability (Section 2.1.2) underpins various graphical diagnostics. If X_1, \dots, X_n follow $\text{GP}(\sigma, \xi)$ above a threshold u , and $\xi < 1$, then

$$e(v) = \mathbb{E}(X - v \mid X > v) = \frac{\sigma_u - \xi u}{1 - \xi} + \frac{\xi}{1 - \xi} v, \quad v \geq u. \quad (12)$$

This motivates the mean excess, or mean residual life, plot (cf. Davison and Smith, 1990, § 2), which graphs the empirical mean excesses $\hat{e}(v) = n_v^{-1} \sum_{i=1}^{n_v} (X_i - v)_+$ against thresholds v in a grid \mathcal{U} , in the hope that the graph will become roughly straight above some threshold. Its interpretation is aided by supplementing the graph with uncertainty bands.

Langousis et al. (2016, Section 2.2) proposed automating this informal procedure by taking order statistics as candidate thresholds. Their idea is that for each $u \in \mathcal{U} = \{Y_{(1)} \leq \dots \leq Y_{(n-20)}\}$, a weighted linear regression should be fitted to pairs $\{Y_{(i)}, \hat{e}(Y_{(i)})\}$ ($i = 1, \dots, n - 10$), with j th largest order statistic weighted by the reciprocal sample variance of exceedances over u . The procedure returns the threshold that minimises the weighted mean squared error. Discarding the ten largest order statistics ensures that the weights are not too large, as can arise if there are (near) ties in the largest observations.

The left-hand panel of Figure 2 shows the mean residual life plot for the Padova data with \mathcal{U} consisting of quantiles at levels 0.8 (13.58mm) to 0.995 (65.49mm) in increments of

0.005; there are 663 and 17 exceedances at the limiting values of u . The plot seems to stabilize towards 50mm, but the [Langousis et al. \(2016\)](#) procedure returns the lowest candidate threshold, despite the fitted regression line lying below all observations above 40mm.

3.2 Parameter stability plots

Another popular visual procedure is the parameter stability plot ([Davison and Smith, 1990](#)). If the generalized Pareto model holds above u , then the shape ξ and/or the modified scale $\sigma_v - \xi v$ are constant for $v \geq u$, suggesting that we check for stability of point estimates for values of v in a grid \mathcal{U} , with these estimates supplemented by appropriate confidence intervals. Such plots can be difficult to interpret because the estimates are based on overlapping samples and do not account for penultimate effects. Moreover they provide no assurance that the model fits adequately, so they should be complemented with diagnostics of fit focused on the upper tail. In an attempt to automate such diagnostics by mimicking common practice, in our simulation study we return the lowest threshold u for which the shape parameter estimate at all higher thresholds falls within the confidence interval of ξ at u . Unless there are strong penultimate effects, this leads to the selection of very low thresholds.

The parameter stability plot in the central panel of [Figure 2](#) gives much lower shape estimates than Hill's estimator. There is an initial increase of $\hat{\xi}$ until $u = 40$ or so, but the substantial uncertainty implies that the smallest candidate threshold would be adequate.

3.3 Hill plots

Hill plots graph the Hill estimator H_{n,n_u} of eq. (10) against the number of order statistics n_u used for estimation. The usual recommendation is to choose a number of order statistics n_u in a region where the Hill estimator stabilizes based on visual inspection of pairs (n_u, H_{n,n_u}) for different values of n_u . This is notoriously difficult because the sample paths of the process $\{n_u, H_{n,n_u}\}$ are analogous to those of a modified Brownian motion ([Mason and Turova, 1994](#)) and can be very rough; see [Figure 1](#). The estimates are best graphed against the log number of exceedances and may be smoothed using a moving window estimator. [Resnick \(2006, §§4.4–4.6\)](#) describes alternative Hill plots, including ones in which H_{n,n_u} is replaced by a local average. [Danielsson et al. \(2019\)](#) suggest automating the selection of n_u by looking for a drop in the variance of the Hill estimator. They use the proportion of the m subsequent tail indexes, say $1/H_{n,n_u+1}, \dots, 1/H_{n,n_u+m}$, that lie at most ε from $1/H_{n,n_u}$, suggesting setting $\varepsilon = 0.3$ and taking the largest value of n_u such that 90% of the observations are within the bound. This does not account for the correlation between estimates, and the fact that the variance of the tail index depends on both ξ and n_u .

The right-hand panel of [Figure 2](#) shows the Hill plot, graphed as recommended against $\log_{10} n_u$, for $20 \leq n_u < 663$. Its estimates of ξ are much higher, and seem stable for $n_u \lesssim 150$. The result of the [Danielsson et al. \(2019\)](#) procedure depends on how the range of order statistics is restricted, returning a threshold at 47.6mm with $\hat{\xi} = 0.29$, and $n_u = 54$ if all the non-zero rainfall data are retained, but giving $n_u = 20$ and $\hat{\xi} = 0.28$ above the 0.995 quantile, if n_u is restricted to be less than 1000.

3.4 Likelihood-based procedures

Stability diagnostics can be based on the large-sample distribution of the maximum likelihood estimator. [Thompson et al. \(2009\)](#) suggest performing Pearson's test of normality for differences of the successive estimators $\hat{\sigma}_j - \hat{\xi}_j u_j$ of the scale parameter of the Poisson process model for thresholds u_j in a fixed grid \mathcal{U} , stopping when the hypothesis is rejected at level $\alpha = 0.2$. If the model applies, then these differences should have mean zero, but their correlation complicates the assessment of significance for the tests.

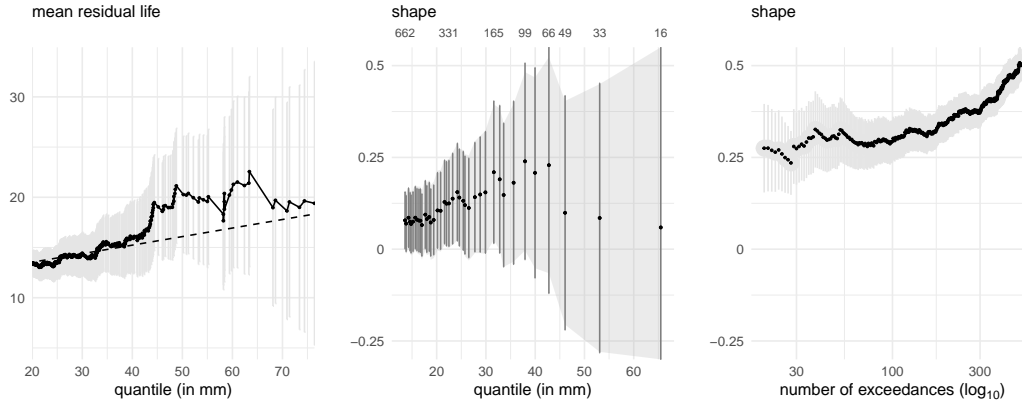


Figure 2 Stability plots for the Padova summer rainfall data, with point estimates as a function of the threshold or the number of exceedances, and 95% Wald pointwise (line segment) and simultaneous (shaded area) confidence intervals. Left: mean residual life from eq. (12), with weighted regression line. Center: stability plot for the shape parameter with pointwise (line) and simultaneous intervals; number of exceedances for selected threshold is shown on top. Right: Hill estimates of the shape parameter against the \log_{10} of the number of exceedances.

Wadsworth (2016) supposes that Poisson processes of the form described in Section 2.1.3 apply with possibly different parameters on each interval of \mathcal{U} , and shows that, if the asymptotic regime with a common shape parameter has been reached, differences of the estimators $\hat{\xi}_1, \dots, \hat{\xi}_J$ based on the exceedances of consecutive thresholds can be rescaled to form asymptotically independent standard normal variables, $\varepsilon_j = (\hat{\xi}_{j+1} - \hat{\xi}_j) / \{(I_{j+1}^{-1} - I_j^{-1})_{\xi, \xi}^{1/2}\}$, for $j = 1, \dots, J - 1$; here I_j is the Fisher information matrix for exceedances of threshold u_j , and the subscript (ξ, ξ) denotes the corresponding matrix element. Her idea is that this standardisation to Gaussian white noise should be effective within the asymptotic regime, but that the ε_j can be treated as Gaussian white noise with another mean and variance at thresholds below this regime. Thus a likelihood ratio test for a changepoint in the distribution of $\varepsilon_1, \dots, \varepsilon_{J-1}$ should indicate the start of the asymptotic regime, as shown by the lowest threshold above which the p -value for the test exceeds some level α . Experience suggests that this procedure is fragile; in particular the difference in inverse Fisher information matrices is often not positive definite, and altering \mathcal{U} can lead to completely different conclusions. The left-hand panel of Figure 3 shows the Wadsworth (2016) white-noise sequence ε_j , which suggests picking the lowest possible threshold for the Padova data.

4 Extended models

The fitting of asymptotic models such as the generalized Pareto distribution to a small subset of the available data, sometimes called the *extremal paradigm*, is the dominant approach to the modelling of rare events, but it has drawbacks. One is that the sharp division of the data into ‘extreme’ and ‘bulk’ at a threshold is unrealistic. A smoother transition towards the tail might be achieved by modifying the generalized Pareto model so that its upper-tail properties remain satisfied in the limit but it is more flexible near the threshold, which could then be lowered without serious misspecification. The goal is to balance potential gains in precision of estimation due to including more data against increased uncertainty due to estimating additional parameters. In this section we describe the main approaches to extending the generalized Pareto distribution and discuss corresponding threshold choice procedures.

4.1 Piecewise generalized Pareto models

In Section 2.1.1 we saw that the penultimate shape parameter typically depends on the threshold. Wadsworth and Tawn (2012) propose approximating this behaviour using a two-phase inhomogeneous Poisson process with different measures of the form of eq. (7) on intervals $(u_1, u_2]$ and $(u_2, +\infty)$. The intensity functions are constrained to be continuous at u_2 , and tests for equality of the two shape parameters are performed at each pair (u_1, u_2) in a fixed grid. The models can be hard to fit, and the procedure entails multiple testing.

Northrop and Coleman (2014) instead propose fitting a piecewise generalized Pareto distribution, $\text{PGP}(\sigma, \xi_1, \dots, \xi_J)$, which consists of interval-truncated GPDs with potentially different shape parameters on the intervals defined by a fixed grid $\mathcal{U} \cup \{+\infty\}$. Continuity of the density function at u_2, \dots, u_J imposes $J - 1$ restrictions on the scale parameters, so the full model has only $J + 1$ parameters. The model can be challenging to fit, so the authors propose score tests of the hypotheses that $\xi_j = \dots = \xi_J$, which correspond to a single generalized Pareto model above u_j , against the alternative that ξ_j, \dots, ξ_J are different. They plot the corresponding p -values against the thresholds, and for a given significance level α then choose the lowest threshold with a non-significant p -value or at which the p -values for all higher thresholds are all non-significant. The central panel of Figure 3, which shows this plot for the Padova data, leads to the choice of the 0.8 quantile as threshold.

Under the original Northrop–Coleman procedure, the rejection probability at any particular threshold is α , but the tests are dependent because the data are re-used. Moreover, its power depends on \mathcal{U} and especially on u_J . Neither of their proposed approaches to choosing a threshold controls the overall error rate: the sequence of p -values does not allow comparison of the null models across thresholds because the data differ for each test. An alternative procedure tests a $\text{PGP}(\sigma, \xi_1, \dots, \xi_J)$ model with $\xi_j = \dots = \xi_J$ for $j = 1, \dots, J - 1$ against the full piecewise model using likelihood ratio statistics with $J - j$ degrees of freedom. As the data do not change, this also allows model comparison using information criteria. This entails full fits of J models, first fitting the ordinary generalized Pareto model to all the data above u_1 , then successively fitting the models with $\xi_1 \neq \dots \neq \xi_j = \dots = \xi_J$ for $j = 2, \dots, J$, using the final parameter values for one fit as starting-values for the next; this is more stable and faster than direct fitting of the full model. The likelihood will increase when each parameter is added, but the full model remains quite difficult to fit and the shape parameter estimates can vary appreciably between successive intervals.

4.2 Extended generalized Pareto models

Starting from Papastathopoulos and Tawn (2013), numerous attempts have been made to embed the GP distribution function $G(x; \sigma, \xi)$ in a more flexible model without changing its limiting tail behaviour. Apart from the hope of being able to use a lower threshold for inference on the upper tail, or even entirely avoiding choosing a threshold, this approach may also allow the simultaneous modelling of extremes in both tails (Naveau et al., 2016). A general construction of such models rests on a continuous distribution function F_κ on $[0, 1]$, whose density is f_κ . The $\text{EGP}(\sigma, \xi, G_\kappa)$ distribution function is then (Naveau, 2025)

$$\Pr(X \leq x) = F_\kappa\{G(x; \sigma, \xi)\},$$

and the corresponding density and quantile functions are

$$f(x; \sigma, \xi) f_\kappa\{G(x; \sigma, \xi)\}, \quad \sigma Q_\xi\{f_\kappa^{-1}(p)\}, \quad 0 < p < 1,$$

where $Q_\xi(p) = \{(1 - p)^{-\xi} - 1\}/\xi$ for $\xi \neq 0$ and $Q_0(p) = -\log(1 - p)$ is the generalized Pareto quantile function.

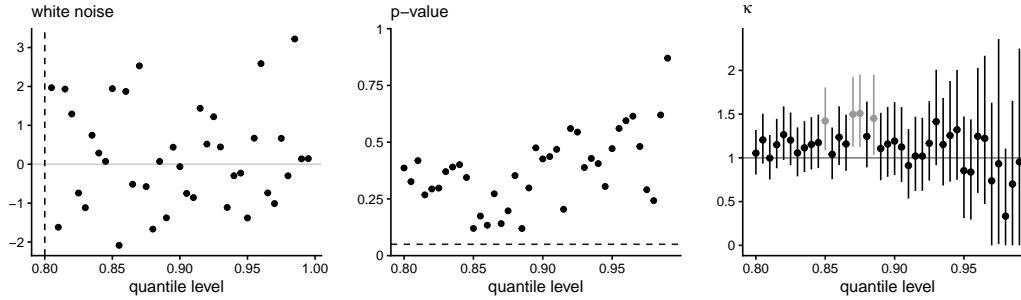


Figure 3 Threshold selection diagnostics for the Padova rainfall series. Left: white noise sequence diagnostic of Wadsworth (2016) from Section 3.4; rescaled differences of shape parameter estimates, $\{\xi_i^*\}$. The dashed vertical line indicates the lowest threshold at which we fail to reject the hypothesis that the sequence is standard Gaussian white noise. Center: p-values of the Northrop and Coleman (2014) score test against threshold. The horizontal dashed line at $\alpha = 5\%$ gives the cutoff for individual tests. Right: parameter stability plot for κ for the beta extended generalized Pareto model (Gamet and Jalbert, 2022), with pointwise profile-based 95% confidence intervals. Intervals that fail to cover $\kappa = 1$ are in grey.

Extended generalized Pareto distributions provide more flexibility for modelling departures from the limiting form, and thus may allow a user to choose lower thresholds and increase the sample size, while allowing the additional parameters to capture departures from a generalized Pareto tail for lowest exceedances. In the case of scalar κ , with $\kappa = a$ retrieving the generalized Pareto model, parameter stability plots can be used to find a region in which $\kappa \approx a$ and the shape parameter stabilizes. Hypothesis tests for $\kappa = a$ can also be constructed, although testing will only be regular if a lies inside the parameter space. However, estimators of κ are typically strongly correlated with those of (σ, ξ) , so parameter uncertainty balloons, even if that for return levels increases less sharply. Huet, Naveau and Sabourin (2026) proposed fitting an extended generalized Pareto model to (a subset of the) data and picking the largest point above which the density is convex as threshold (the largest zero of the second derivative of the density $\arg \max_x \partial^2 f(x; \theta) / \partial x^2 = 0$). This is justified by the fact that the generalized Pareto density is strictly convex when $\xi > -1/2$, and both models should behave similarly in the tail. As EGD models are appropriate only for positive data, this procedure anyway requires the set of exceedances of an initial threshold.

The Papastathopoulos and Tawn (2013) models have prescribed behaviour at $x = 0$: for example, if $F_\kappa = u^\kappa$ for $\kappa > 0$, the density at the origin is $g(0; \sigma, \xi) = 1/\sigma$ but $f_\kappa(0)$ equals zero if $\kappa > 1$ or $+\infty$ if $\kappa < 1$. Gamet and Jalbert (2022) propose two further models that avoid this behaviour, but only their extended beta model leads to regular asymptotics for comparisons with the generalized Pareto. Stein (2021) considers other constructions.

Parameter stability plots for κ for the Padova data and the Gamet and Jalbert (2022) beta model, shown in the right-hand panel of Figure 3, suggest no evidence against the generalized Pareto model from the 0.88 quantile onwards, perhaps due to a lack of power. The estimator of κ is highly correlated with that of ξ , which leads to wide confidence intervals and complicates assessment. The 100-year return levels from fitting different extended generalized Pareto models to these data at different thresholds yield essentially the same inference, although the upper bound of the confidence interval associated with the EGP model tends to be higher, most likely owing to the added uncertainty due to expanding the model class. The two extended generalized Pareto models, the beta model of Gamet and Jalbert (2022) and the power model of Papastathopoulos and Tawn (2013) exhibit similar behaviour for the sampling distribution of the return level estimator. The Huet, Naveau and Sabourin (2026) procedure returns a threshold of zero based on the entire Padova rainfall series, as the EGP fit

is convex over the whole domain, with $\hat{\xi} \approx 0.25$; depending on the lower bound considered for fitting the EGP, we can however obtain very different thresholds.

4.3 Mixture and splicing models

The generalized Pareto model is only valid for exceedances above the threshold u , so it is tempting to splice it together with a specification for the bulk of the data, which lies below u . Section 6 of [Scarrott and MacDonald \(2012\)](#) and the discussion in [Hu and Scarrott \(2018\)](#) outline the ideas in the many papers that take this approach; the latter also provides advice and a software implementation. These methods typically do not consider threshold selection, so are not compared in our simulations, but for completeness we sketch them here.

The distribution function of a “bulk model-based tail fraction” splicing model has disjoint components below and above u with GPD $G(x; \sigma_u, \xi)$ ([Hu and Scarrott, 2018](#)),

$$F(y; \boldsymbol{\theta}) = \begin{cases} H(y; \boldsymbol{\theta}), & y \leq u, \\ H(u; \boldsymbol{\theta}) + \{1 - H(u; \boldsymbol{\theta})\} G(y - u; \sigma_u, \xi), & y > u, \end{cases}$$

where H is the distribution function of the bulk, whereas a “parametrized tail fraction” model uses a mixture of truncated distributions with mixing probability ϕ_u ,

$$F(y; \boldsymbol{\theta}) = \begin{cases} (1 - \phi_u)H(y; \boldsymbol{\theta})/H(u; \boldsymbol{\theta}), & y \leq u, \\ (1 - \phi_u) + \phi_u G(y - u, \sigma_u, \xi), & y > u. \end{cases}$$

The second specification is more flexible and its likelihood factorises, so it is preferable unless the bulk model fits well: this can be assessed using standard diagnostic tools.

Splicing models describe the whole distribution, so users can treat u as a parameter and choose it to give the best fit; its uncertainty can also be taken into account. On the other hand the resulting estimate may be unduly influenced by the bulk model, so robustness of the fit to the choice of u is critical. Goodness-of-fit measures, such as quantile-quantile plots for both parts of the distribution, are often helpful. Profile likelihoods for u can sometimes be plotted, but they are typically uninformative and multimodal: the central panel of [Figure 4](#) shows profile log-likelihood functions for the threshold based on various mixture models for the Padova data, which, though unstable, all point to a low threshold. Using the bulk model-based rather than the parametrized tail fraction does not change the overall picture, but the profiles are smooth when continuity is imposed at u . Neither Weibull (threshold at 0.855 quantile) nor gamma (threshold at quantile 0.8) models fit the bulk adequately, but quantile-quantile plots (not shown) show satisfactory fit in the tails, with shape estimates of respectively 0.08 and 0.16 for the GP component.

Continuity of parametric models can be imposed by equating the density, and perhaps its derivatives, at the threshold. This leads to more natural-looking models, but the resulting interaction between the bulk and tail models can lead to poor quantile estimation if either part fits badly. [Carreau and Bengio \(2009\)](#) consider a Gaussian-generalized Pareto splicing model, imposing continuity on the density and its derivative at u , which is treated as a free parameter defined implicitly through the constraints or by constrained optimisation. [Rivera Mancía \(2014\)](#) consider similar smoothness constraints and a Bayesian nonparametric mixture for the generalized Pareto tail model, while [MacDonald et al. \(2011\)](#) use kernel density estimation with a continuity constraint for the bulk, with the kernel bandwidth chosen using a cross-validated likelihood. [do Nascimento, Gamerman and Lopes \(2012\)](#) consider a discontinuous model in the Bayesian paradigm and argue that the discontinuity has no impact for posterior predictive inference about the tail if u is treated as random.

Many papers have considered Bayesian estimation, as careful prior specification can help deal with multimodal likelihood functions and capture the uncertainty in threshold selection.

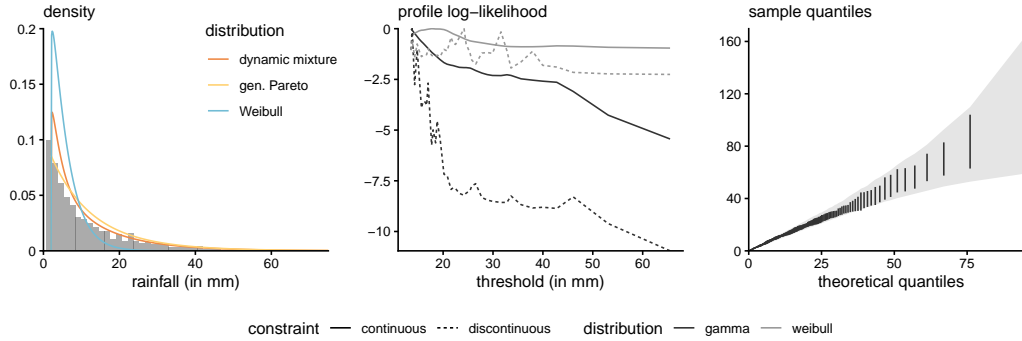


Figure 4 Splicing and dynamic mixture models for the Padova data, and threshold selection diagnostics. Left: dynamic Weibull-generalized Pareto mixture density of *Frigessi, Haug and Rue (2002)*. Center: profile log-likelihood functions for the threshold parameter u for Weibull and gamma splicing models, with and without continuity constraints at the threshold. Right: quantile-quantile plot for the *Murphy, Tawn and Varty (2025)* procedure at the selected threshold of $u = 13.58\text{mm}$, corresponding to the 0.8 quantile, with tolerance bands (grey) and segments giving the approximate positions of observations, all of which fall within the bands.

For example, *Behrens, Lopes and Gamerman (2004)* considered splicing models where u is treated as a model parameter, with a left-truncated distribution centered around high quantiles as its prior, and *de Zea Bermudez, Amaral Turkman and Turkman (2001)* confine the threshold to a reasonable range by using a doubly-truncated Poisson prior for the number of exceedances. *Tancredi, Anderson and O’Hagan (2006)* used the inhomogeneous point process parametrization to reduce dependence on the threshold.

Splicing mixtures in which the bulk is nonparametrically specified, using a Dirichlet process mixture of gamma densities, a mixture of uniform densities or kernel density model, are more flexible than their parametric counterparts, but are more computationally demanding and convergence can be problematic; Chapter 5 of *MacDonald (2011)* considers the use of Tukey’s sensitivity curves for maximum likelihood estimators of the extremal mixture parameter, when transferring data between bulk and tail.

Splicing and extended generalized Pareto distributions can be combined by smoothly blending the bulk and tail through a transition function that allows the weight in the mixture density to vary dynamically (*Frigessi, Haug and Rue, 2002*), with

$$f(y) \propto \{1 - w(y; \boldsymbol{\vartheta})\}h(y; \boldsymbol{\theta}) + w(y; \boldsymbol{\vartheta})g(y; \sigma, \xi),$$

and the weighting function $w(\cdot)$ taken to be a location-scale Cauchy distribution function. Here the bulk and tail models are defined over the whole real line, with the tail given by a dynamic weighted mixture. Since the parameters of w govern the mixing weight, there is no guarantee that the generalized Pareto model will dominate in the upper tail, and this approach tends to perform poorly in practice. *Scarrott and MacDonald (2012)* remark that a transition function with a high density in a small neighborhood yields sharp transitions. The left-hand panel of Figure 4 shows the fit of the *Frigessi, Haug and Rue (2002)* dynamic mixture model to the Padova rainfall totals greater than 2mm. The generalized Pareto shape parameter takes the reasonable value of 0.06, but the tail model contributes 50% of the weight from the minimum exceedance onwards, indicating possible contamination of the tail by the bulk.

5 Goodness-of-fit measures

Threshold stability plots do not measure the fit of the tail model to the data, making it hard to assess whether inference and subsequent extrapolation are reliable. Another natural approach is to base threshold selection on the fit of a generalized Pareto model to the tail data.

5.1 Quantile-quantile plot distance

The fit of data to a distribution F_0 is often assessed using quantile-quantile (Q-Q) plots of ordered data against plotting positions, typically $\{p_j = j/(n+1) : j = 1, \dots, n\}$, that have been transformed using the quantile function Q_0 of F_0 . When the shape of F_0 depends on parameters, as with the GPD, uncertainty can be assessed by parametric simulation from a fitted distribution \hat{F}_0 (Davison and Hinkley, 1997, §4.2.4). The model is refitted to each simulated sample and the corresponding quantile function is evaluated at the plotting positions.

To avoid visual inspection of Q-Q plots for a grid of thresholds, Varty et al. (2021) suggest using a metric such as (weighted) mean absolute or mean square error for agreement of the empirical and theoretical positions. Murphy, Tawn and Varty (2025) suggest fixing grids \mathcal{U} of thresholds and $\mathcal{P} = \{p_1, \dots, p_m\}$ of plotting points at which to evaluate the fit and using a bootstrap scheme for $u \in \mathcal{U}$:

- for $b = 1, \dots, B$, generate bootstrap samples of exceedances of u and obtain the corresponding fitted GP models $\hat{F}_0^{(b)}$;
- obtain the x -axis positions using the generalized Pareto quantile function for $\hat{F}_0^{(b)}$, evaluated at \mathcal{P} ;
- obtain the y -axis positions from the empirical quantile function evaluated at \mathcal{P} ;
- compute the average metric over \mathcal{P} and the B bootstrap samples.

The threshold u giving the smallest average metric is chosen. By modifying the sampling scheme this proposal can be used with censored or non-identically distributed data, and for time-varying thresholds, but it requires an optimization for each bootstrap sample and each threshold. Varty et al. (2021) propose using a nonparametric bootstrap and plotting on the exponential scale with l_1 norm as metric, whereas Murphy, Tawn and Varty (2025) compute the metric on the generalized Pareto scale. The latter gives lower mean squared error for quantile estimators when the shape ξ is positive, since the exponential model downweights larger observations and leads to the choice of lower thresholds. The TAILS approach of Collings et al. (2025), who suggest assigning more weight to large values of \mathcal{P} and discarding those below a user-selected cutoff p_0 , leads to the selection of much higher thresholds.

Murphy, Tawn and Varty (2025) report simulation studies that suggest reduced root mean squared error for their quantile estimators relative to the procedures of Northrop, Attalides and Jonathan (2017) and Wadsworth (2016). Using this with the l_1 norm on the Padova data returns the lowest candidate threshold; the quantile-quantile plot in the right-hand panel of Figure 4 shows a good fit, but very wide uncertainty for the highest quantiles.

5.2 Minimum distance selection

A popular approach for fitting to network data exhibiting power-law upper tails (Clauset, Shalizi and Newman, 2009) treats observations above u as an exact sample from a Pareto distribution with survival function $(x/u)^{-1/\xi}$ on $[u, \infty)$. They suggest picking the threshold u to minimize the Kolmogorov–Smirnov distance between the empirical distribution function of the exceedances, \hat{F}_{n_u} and the best fitting Pareto model obtained using Hill’s estimator, and assess uncertainty using a nonparametric bootstrap. Drees et al. (2020) consider

candidate thresholds among the order statistics and show that the resulting shape parameter estimator has a higher asymptotic mean squared error than Hill's estimator and that the chosen thresholds tend to be higher than would be optimum. A related proposal of [Danielsson et al. \(2019\)](#) suggests picking n_u to minimize the supremum distance between [Weissman \(1978\)](#)'s quantile estimator and the empirical quantile of the largest exceedances, but simulations of [Murphy, Tawn and Varty \(2025\)](#) suggest that this has high bias that leads to overly high thresholds, due both to the chosen criterion and to not accounting for the variability of the order statistics. For Pareto tails with $\xi > 0$, [Goegebeur, Beirlant and de Wet \(2008\)](#) also mention choosing n_u to minimize a weighted Cramér–von Mises statistic between log exceedances and the fitted exponential quantiles.

5.3 Bootstrap procedure

To account for variation in the number of exceedances above a fixed threshold u , one can employ a bootstrap procedure. We estimate as usual the parameters σ_u, ξ of the generalized Pareto distribution from eq. (2) from the n_u exceedances of a threshold u , and consider the mixture distribution function consisting of point mass at observed values and a generalized Pareto tail

$$\tilde{F}(y) = \frac{1}{n} \sum_{i=1}^{n-n_u} \mathbf{1}_{Y_{(i)} \leq y} + \mathbf{1}_{u < y} \frac{n_u}{n} G(y - u, \hat{\sigma}_u, \hat{\xi}). \quad (13)$$

A bootstrap sample is drawn by taking n uniform draws and inverting eq. (13), leading to varying numbers of exceedances above u , to which the generalized Pareto model is fitted.

[Caers, Beirlant and Maes \(1999\)](#) suggest minimizing the mean squared error of the shape parameter, which they estimate from the discrepancies between the resulting bootstrap shape estimates and the original estimate value $\hat{\xi}$. In practice, the variance tends to dominate the bias, so this approach leads to low thresholds. [Gonzalo and Olmo \(2004\)](#) propose checking the fit of the generalized Pareto model using a Kolmogorov–Smirnov statistic that compares the empirical distribution function and fitted GPD, generalizing [Pickands \(1975\)](#), and to use the bootstrap based on eq. (13) to approximate its sampling distribution.

5.4 Methods based on L -moments

The scale-invariance of L -moment ratios, $\tau_r = \lambda_r / \lambda_2$ ($r = 3, \dots$) (Section 2.2.3), can be used to evaluate distributional fit. [Silva Lomba and Fraga Alves \(2020\)](#) propose automating visual selection from plots of these ratios by noting that the L -skewness $\tau_3 = (1 + \xi) / (3 - \xi)$ of the generalized Pareto distribution is related to its L -kurtosis, $\tau_4 = f(\tau_3) = \tau_3(1 + 5\tau_3) / (5 + \tau_3)$. Their idea is to compare their empirical estimates $(\hat{\tau}_3, \hat{\tau}_4)$ and the implied L -moments $\{\hat{\tau}_3, f(\hat{\tau}_3)\}$ on a plot of τ_4 against τ_3 for $u \in \mathcal{U}$, then choose the threshold u to minimise the l_2 distance to the theoretical curve, i.e., taking

$$\hat{u} = \operatorname{argmin}_u \min_{\tau_3} \{ \hat{\tau}_3(u) - \tau_3 \}^2 + \{ \hat{\tau}_4(u) - f(\tau_3) \}^2.$$

[Kiran and Srinivas \(2021\)](#) likewise propose fitting the generalized Pareto distribution to the exceedances of u , mapping them using the probability integral transform to the unit exponential scale and calculating the first L -moment and L -skewness, $(\hat{\lambda}_1, \hat{\tau}_3)$, from the transformed sample. They then use Monte Carlo sampling from unit exponential or analytical approximation to estimate the mean and variance matrix of these estimators, and return the threshold that minimises the Mahalanobis distance between $(\hat{\lambda}_1, \hat{\tau}_3)$ and the “theoretical” values for the unit exponential model, found by simulation.

Solari et al. (2017) use the weighted Anderson–Darling statistic of Sinclair, Spurr and Ahmad (1990),

$$A_R^2(\mathbf{y}) = \frac{n_u}{2} - \sum_{i=1}^{n_u} \left\{ \frac{2n_u - 2i + 1}{n_u} \log(1 - z_i) + 2z_i \right\},$$

for each candidate threshold u and corresponding set of n_u exceedances, where $z_i = G(y_{(n_u+1-i)} - u; \hat{\sigma}_u, \hat{\xi})$, with G the distribution function of eq. (2) using the L -moment estimates $(\hat{\sigma}_u, \hat{\xi})$. The null distribution of A_R^2 is approximated by parametric bootstrap simulation. Solari et al. (2017) recommend choosing the threshold for which the p -value for A_R^2 is highest, but this would lead to random selection if the data were exactly generalized Pareto.

5.5 Bayesian predictive measures

Lee, Fan and Sisson (2015) propose a threshold stability plot that shows the Bayesian p -value for a summary statistic that captures the agreement or ‘surprise’ between sample and data simulated from the posterior distribution. Too low a threshold will be suggested by departures from the expected value of 0.5 for p -values, which are uniform if the GPD fits well. Samples from the posterior distribution of the generalized Pareto parameters (σ, ξ) are then used to compute the test statistic for the observed exceedances and simulated posterior predictive samples. Lee, Fan and Sisson (2015) make box-and-whisker plots of p -values, so the procedure must be replicated to provide decent Monte Carlo estimates of the variability. The results are noisy even with data simulated from the null model, making it hard to diagnose lack of fit. Furthermore, there is some arbitrariness in the choice of goodness-of-fit statistic. The partial posterior predictive distribution is based on the posterior conditional on the statistic, and is equivalent to a leave-one-out scheme if the statistic considered is the posterior log density of the r th order statistic. This choice yields overly-variable p -values, visible in simulations of Lee, Fan and Sisson (2015). More work seems to be needed on appropriate measures of surprise and to reduce the computational burden.

The left-hand panel of Figure 5 shows measures of surprise for the Padova data using the likelihood of the largest order statistic as validation test statistic and simulating samples from the partial posterior predictive distribution, and using the the reciprocal likelihood based on the full posterior. The former suggests that all thresholds are unsuitable, the latter that the lowest possible threshold would be suitable. It is unclear whether the reciprocal likelihood lacks power to detect poor fit.

Northrop, Attalides and Jonathan (2017) propose a Bayesian method based on leave-one-out cross-validation with a binomial-generalized Pareto (BGP) model, whose density for $\tau_u = \Pr(Y > u)$ is

$$f_u(y) = (1 - \tau_u)^{\mathbf{1}_{y \leq u}} \{ \tau_u g(y - u; \sigma_u, \xi) \}^{\mathbf{1}_{y > u}}.$$

They use a fixed grid \mathcal{U} and a validation threshold $v > u_j$ above which they assess model performance: the BGP model above v follows from threshold-stability arguments, with corresponding likelihood contribution f_v . The ‘cross-validation predictive density’ for the left-out observation x_r from $\mathbf{x}_{-r} = \{x_1, \dots, x_{n_{u_j}}\} \setminus \{x_r\}$, the full sample of exceedances minus the r th observation exceeding candidate threshold u_j , is

$$f_v(x_r | \mathbf{x}_{-r}, u_j) = \int f_v(x_r | \boldsymbol{\theta}, \mathbf{x}_{-r}) p_j(\boldsymbol{\theta} | \mathbf{x}_{-r}) d\boldsymbol{\theta},$$

with p_j the posterior density of the parameters at threshold u_j . The cross-validation predictive density, $f_v(x_r | \mathbf{x}_{-r}, u_j)$, is approximated using Monte Carlo samples from $p_i(\boldsymbol{\theta} | \mathbf{x}_{-r})$

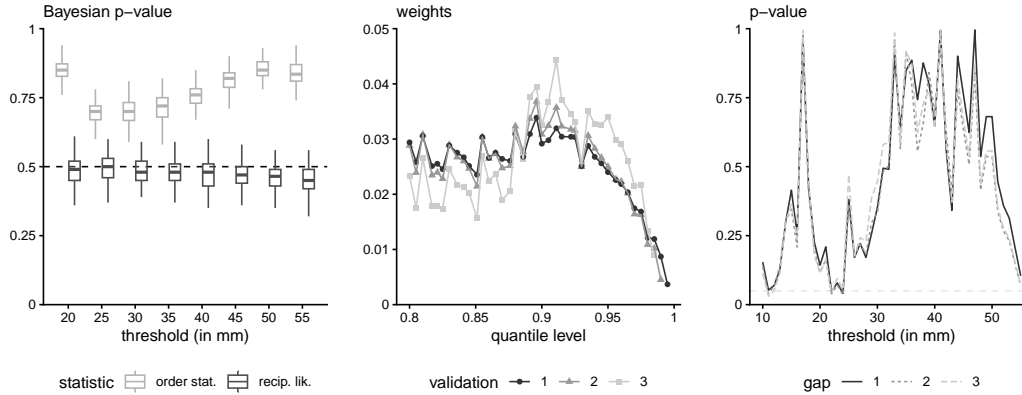


Figure 5 Threshold selection diagnostics for the Padova rainfall series. Left: [Lee, Fan and Sisson \(2015\)](#) measures of surprise (Section 5.5) with two test statistics, the reciprocal likelihood $1/f(\mathbf{x}; \boldsymbol{\theta})$ or equivalently $-\ell(\boldsymbol{\theta}; \mathbf{x})$ and the distribution of the largest order statistic, $X_{(n)}$. The box-and-whiskers plots are based on 100 replications at each threshold. Center: model averaging weights obtained by Bayesian leave-one cross-validation using the top order statistics as validation threshold ([Northrop, Attalides and Jonathan, 2017](#)). Right: p-values for the information matrix test of [Sèveges and Davison \(2010\)](#) as a function of the maximum gap length $K = 1, \dots, 3$.

obtained via importance sampling from the full posterior $p_j(\boldsymbol{\theta} | \mathbf{x})$. The proposed measure of fit, an estimate of the negative Kullback–Leibler divergence,

$$\hat{T}_v(u_j) = \sum_{r=1}^{n_{u_j}} \log \hat{f}_v(x_r | \mathbf{x}_{-r}, u_j),$$

uses all exceedances to assess fit, unlike in [Lee, Fan and Sisson \(2015\)](#). The selected threshold maximizes this diagnostic over \mathcal{U} . [Northrop, Attalides and Jonathan \(2017\)](#) use Bayesian model averaging to account for the uncertainty due to threshold selection, with the prior predictive distribution replaced by the proxy $\exp\{\hat{T}_v(u_j)\}$; weights as a function of the threshold are shown in the central panel of Figure 5 for validation based on up to the three largest candidate thresholds. The approach is computationally-intensive but the choice of threshold is automatic and is based on the fit of the model. The BGP likelihood allows the comparison of different thresholds, but does not provide a valid joint distribution for the whole sample above the lowest threshold; this seems to impact comparisons of predictive fit. Simulations in [Murphy, Tawn and Varty \(2025\)](#) indicate that the method leads to highly variable threshold choices, and we concur with this.

5.6 Distributional tests

One way to automate threshold selection is to fit a generalized Pareto distribution at each threshold in a fixed grid \mathcal{U} , compute a goodness-of-fit statistic, and then perform tests sequentially for $u \in \mathcal{U}$ until rejection. [Choulakian and Stephens \(2001\)](#) considered Anderson–Darling and Cramér–von Mises statistics for testing whether the data above a threshold are generalized Pareto. They tabulated the null distributions of these statistics, which do not depend on the scale parameter, though [Langousis et al. \(2016\)](#) point out that these distributions are valid only for unrounded data and that their validity suffers further under serial correlation. [Bader, Yan and Zhang \(2018\)](#) proposed an improved approach using Monte Carlo simulation to approximate the null distribution for more values of the shape parameter, with linear extrapolation for the largest values of the test statistic. Although invalid in this setting, ForwardStop ([G’Sell et al., 2016](#)) is used in a bid to control the false positive rate and thus

to alleviate multiple testing concerns. Bader, Yan and Zhang (2018) suggest using the p -values for a goodness-of-fit statistic at each threshold in a fixed grid \mathcal{U} to form the sequence $D_j = -j^{-1} \sum_{i=1}^j \log(1 - P_i)$ ($j = 1, \dots, J$) and choosing the largest threshold for which $D_j < \alpha$. Simulation suggests that the Anderson–Darling statistic gives higher power than other statistics considered, and despite the lack of theoretical guarantees for the control of the false discovery rate, the size distortion of the procedure seems to be small. Simulations in their paper suggest that the approach leads to lower mean squared error for prediction of extreme quantiles than the competing methods considered. Adjustments are needed for the null distribution approximation to be reliable with rounded data.

5.7 Time series

Most results so far assume independent data, but clustering of extremes and serial dependence are widespread in applications. Under mild conditions, Ferro and Segers (2003) show that the intervals between successive exceedances of a high threshold u of data from a stationary sequence Y_1, \dots, Y_T approximately follow a mixture of an exponential distribution with rate $\theta\lambda_u$ and a point mass at zero; here λ_u is the rate of exceedances over u and the extremal index $\theta \in (0, 1]$ is the reciprocal of the limiting mean cluster size. Under conditions on extremal clustering, Süveges and Davison (2010) adapt this result and for data with n_u exceedances and intervals T_1, \dots, T_{n_u-1} define the set of truncated intervals $S(u, K) = \{\max\{T_i(u) - K, 0\} : i = 1, \dots, n_u - 1\}$ for possible gaps $K = 0, 1, \dots$, and the corresponding log-likelihood function for θ , $\ell\{\theta; S(u, K)\}$. If the model is well-specified, then for every threshold u_j in a grid \mathcal{U} and gap K , the Fisher information $I(\theta) = -E[\ell''\{\theta; S(u_j, K)\}]$ equals the variance of the score statistic $J(\theta) = \text{Va}[\ell'\{\theta; S(u_j, K)\}]$. Results of White (1982) suggest testing whether $D(\theta) = J(\theta) - I(\theta)$ equals zero, with J and I replaced by their empirical counterparts evaluated at the maximum likelihood estimator and the test statistic compared to its null asymptotic distribution. This procedure gives a p -value for each combination (u_j, K) , and leads to multiple testing. Fukutome, Liniger and Süveges (2015) suggest an *ad hoc* automation that keeps all pairs for which the test statistic is less than 0.05 (i.e., the p -value exceeds 0.82) and choosing the combination of run length and threshold that yields the most clusters; they recommend having at least 80 exceedances at every threshold, but this does not palliate the multiple testing. The application of this to the Padova data in the right-hand panel of Figure 5 shows relative insensitivity to K , and suggests that the model misspecification is not significant beyond 25 mm, giving $n_u = 271$.

6 Semiparametric methods

Threshold selection for moment estimators is typically based on minimizing an asymptotic mean squared error for Hill's estimator, eq. (10). Related methods rely on assumptions about the second-order behaviour of the survival function and the sign of the shape parameter, and may perform poorly in finite samples. Most do not account for the noise due to the insertion of point estimators into formulae, and numerical implementations may not respect the need for a minimum number of upper order statistics, $n - n_u$, for estimation to be reliable, so users must check the results with care.

6.1 Expansions for the asymptotic mean squared error

Caeiro and Gomes (2016) review, but do not numerically compare, semiparametric procedures for positive shape parameters for distributions that are second-order regularly varying;

see our Simulation study 2. These procedures either require values of higher-order parameters that appear in the asymptotic mean squared error formula, which are estimated or fixed, (e.g., setting $\rho = -1$), or use bootstrap schemes to circumvent having to do so.

For the [Hall and Welsh \(1985\)](#) class defined in eq. (6), for example, choosing the intermediate sequence n_u so that $\lambda < \infty$ and the asymptotic mean squared error is $\xi^2/n_u + A^2(n/n_u)/(1-\rho)^2$, gives

$$n_u = \left\lfloor \frac{(1-\rho)^2 n^{-2\rho}}{-2\rho\beta^2} \right\rfloor^{1/(1-2\rho)} \quad (14)$$

as the optimal number of threshold exceedances. This is found by inserting estimates of β and ρ — though the estimation of these second-order quantities requires another choice of intermediate sequence. Algorithm 1 of [Caeiro and Gomes \(2016\)](#) provides a fixed-point iteration scheme to estimate n_u . Since risk measures are typically high quantiles, minimization of the asymptotic mean squared error for estimation of ξ might appear to be inappropriate, but the method appears to be competitive in simulations.

[Dupuis and Victoria-Feser \(2003\)](#) propose selecting the threshold by choosing the number of exceedances n_u that minimizes a weighted prediction error criterion for Pareto tails, and in [Dupuis and Victoria-Feser \(2006\)](#) couple this with robust estimation of the shape parameter, which yield threshold-dependent weights for the observations. We did not implement this latter proposal.

6.2 Bootstrap methods

[Hall \(1990, §4\)](#) was the first to suggest the use of resampling to evaluate the asymptotic mean squared error of Hill's estimator and choose n_u . Taking $m < n$ observations and n_0 initial exceedances, the bootstrap algorithm is as follows:

1. estimate the shape parameter using Hill's estimator with the n_0 largest order statistics;
2. perform B bootstrap replications as follows: resample $m = o(n)$ observations with replacement, compute Hill's estimator for the $n_m = 1, \dots, m$ largest order statistics, and denote the shifted estimates for the b th replicate by $d_{n_m}^{(b)} = (\hat{H}_{m,n_m}^{(b)} - \hat{H}_{n,n_0})^2$;
3. for each value of n_m , average the $d_{n_m}^{(b)}$ over all bootstrap replications, and select the value \hat{n}_m that minimizes the mean squared error.
4. For given ρ , compute the optimal number of exceedances for the full sample, i.e., $\hat{n}_u = \hat{n}_m (n/m)^{-2\rho/(1-2\rho)}$.

The method is sensitive to the choices of n_0 and m , which are left to the user ([Caeiro and Gomes, 2014](#)). Our simulations use the default values of $n_0 = 2n^{1/2}$ and $m = \lfloor n^{0.955} \rfloor$.

The bootstrap procedure requires the index of second-order regular variation to be known or estimated; [Hall \(1990\)](#) took $\rho = -1$. Fixing ρ can be avoided by using a double bootstrap ([Draisma et al., 1999](#)), which requires subsamples of sizes m_1 and $m_2 = n(m_1/n)^\omega < m_1$ with $\omega > 1$. If $\omega = 2$, then $m_2 = m_1^2/n$ and $\hat{n}_u^2(m_1)/\hat{n}_u(m_2) = \hat{n}_u(n)\{1 + o_p(1)\}$ as $n \rightarrow \infty$ ([Gomes and Oliveira, 2001](#)). Ostensibly optimal values of $\hat{n}_u(n)$ may turn out to be larger than n or may equal zero. While some authors suggest independent bootstrap runs, picking m_2 draws from the m_1 samples gives better precision, which might be further improved by bootstrap recycling ([Ventura, 2002](#)). In summary, the optimal choice of $n_u(n)$ is based on the asymptotic relation between the latter and $\hat{n}_u(m_1)$ and $\hat{n}_u(m_2)$; the relationship also yields an estimate of ρ as a by-product.

Other semiparametric shape estimators may have bias properties similar to those of Hill's estimator (cf. [Caeiro and Gomes, 2014](#), and references therein). [Draisma et al. \(1999\)](#) proposed using the double bootstrap for the moment estimator of [Dekkers and de Haan \(1989\)](#),

whereas Danielsson et al. (2001) considered the difference between de Vries' $\hat{\xi}^v$ (de Haan and Peng, 1998) and Hill's estimators. Other choices of intermediate statistics are considered in Gomes and Oliveira (2001), who compare the performance of different bootstrap methods for semiparametric estimation by simulation.

Estimation of second-order parameters can add appreciable variability, so some authors have followed Hall (1990) and fixed ρ . Schneider, Krajina and Krivobokova (2021) proposed the SAMSEE estimator of n_u , obtained by combining the generalized jackknife estimator $2\hat{\xi}_{n,n_u}^v - H_{n,n_u}$ to estimate ξ and a bias estimator obtained from the difference between smoothed Hill estimators over different windows; the result estimates the asymptotic mean squared error for $\rho = -1$. They report that their threshold selection procedure is competitive, with stable performance over a range of sample sizes and heavy-tailed distributions.

Drees and Kaufmann (1998) base threshold selection on calculations of the convergence rate of the maximum random fluctuation of the Hill estimator, $\max_i i^{1/2} |H_{n,i} - \xi - b_{n,i}| = O_p\{\log^{1/2}(\log n)\}$ for the bias $b_{n,i}$, but Caeiro and Gomes (2016) claim that this is sensitive to tuning parameters; in our simulations, it usually failed to return results when using the default values for them, and its performance seems to be subpar.

6.3 Exponential approximations

Under the assumption of regular variation, and with $\xi > 0$, the log-spacings form an approximate exponential sample, so Hill (1975) suggested increasing the number of order statistics until the exponential model is found to be inadequate. As the departure from the theoretical model is very gradual, this typically selects n_u to be too large (Hall and Welsh, 1985).

Guillou and Hall (2001) also consider approximating the distribution of Hill's estimator and a modification thereof based on linear combination of log spacings, obtaining a sum of exponential variables and a bias term to be minimized. The sum of squares of the zero-mean statistic is computed over a moving window and the chosen threshold is the smallest n_u for which the estimate exceeds a critical value.

Beirlant, Vynckier and Teugels (1996b) note that, when the sample exceedances are tail-equivalent to a Pareto distribution, the shape parameter $\xi > 0$ can be viewed as the slope in an exponential quantile-quantile plot with plotting positions $-\log\{j/(n_u + 1)\}$ against order statistics $Y_{(n-j)}$, which leads to the Hill estimator and kernel-weighted variants (Csörgo, Deheuvels and Mason, 1985). Under second-order regular variation with $\rho \leq 0$, they propose finding the value n_u that minimizes

$$\text{MSE}(H_{n,n_u}) = \frac{1}{n_u} \sum_{j=1}^{n_u} w_{j,n_u}^{\text{opt}} \left\{ \log \left(\frac{Y_{(n-j+1)}}{Y_{(n-n_u)}} \right) - H_{n,n_u} \log \left(\frac{n_u + 1}{j} \right) \right\}^2. \quad (15)$$

The weights w_{j,n_u}^{opt} depend on ρ and provide an estimate of the asymptotic mean squared error of the Hill estimator. Beirlant, Vynckier and Teugels (1996b) propose an iterative procedure with an initial estimate of n_u obtained from an unweighted version of eq. (15), estimate ρ from $m > n_u$ order statistics, and then alternate between estimating n_u and ρ . This procedure is generalized to real-valued ξ in Beirlant, Vynckier and Teugels (1996a) using the generalized quantile regression estimator. The weights depend on ξ when it is negative, and the estimator of ρ is erratic and may return positive values. Both m and ρ must be constrained to avoid nonsense output, and, as for any second-order parameter, unrealistically large samples are needed for reliable estimation of ρ . Moreover the optimal weights can be negative, leading to invalid mean squared errors (Gomes and Oliveira, 2001). Sample paths of eq. (15) are variable, and the procedure does not account for the large uncertainty of the MSE estimates.

Still under an assumed Pareto upper tail, Beirlant et al. (1999) propose a nonlinear exponential regression procedure to estimate the scaling sequence, shape and second-order regular

variation parameters based on the asymptotic representation of log-spacings of upper order statistics as independent exponential variables (Beirlant et al., 1999),

$$Z_j = j(\log Y_{(n-j+1)} - \log Y_{(n-j)}) \sim \exp[\xi + b_{n,n_u} \{j/(n_u + 1)\}^{-\rho}], \quad j = 1, \dots, n_u.$$

A similar model is considered in Feuerverger and Hall (1999). The parameters ξ , ρ and b_{n,n_u} can be estimated by maximum likelihood subject to the constraints $\xi > 0$, $\rho < 0$ and $b_{n,n_u} > 0$, perhaps with further constraints on ρ to reduce bias and avoid nonsensical values. Beirlant et al. (2002) consider nonlinear least squares estimators under additive noise by joint estimation and by a two-stage procedure obtained by substituting a consistent estimator of ρ based on n_0 order statistics considering the least-square bias with $\rho = -1$, then estimating other parameters by maximum likelihood. Under the Hall–Welsh class of distributions (6), they derive the optimal n_u as a function of these parameters and scale parameter b , shape ξ and second-order regular variation index ρ . They suggest an ad hoc automation of their approach by looking at the median estimator obtained by applying the formula for $n_0 = 3, \dots, n/2$.

Goegebeur, Beirlant and de Wet (2008) use kernel weighting to derive alternative tail index estimators and use these to approximate the asymptotic mean squared error of the Hill estimator, with a penalty term. Bladt, Albrecher and Beirlant (2020) use the Rényi representation to define lower-trimmed Hill estimators, which include Hill’s estimator as a special case. Focusing on Hall–Welsh distributions, they derive an explicit relationship between the optimal number of exceedances for the Hill and the lower trimmed Hill estimators under second-order regular variation, and recommend taking the number of exceedances that minimizes the average left-trimmed estimator variance, which is smooth and depends less on n_u than does the Hill estimator. They then use the explicit relationship between estimators to find the corresponding n_u for Hill’s estimator, assuming $\rho = -1$. The method crucially depends on the values for n_u selected for the left-trimmed estimator, which they take to be at least $n/5$. Threshold selection is followed by check of Pareto tails using ratio statistics.

6.4 Alternative procedures

The sample paths of the Hill estimator as a function of n_u are non-differentiable, whereas those of the random block maximum estimator proposed by Wager (2014) are infinitely differentiable, thus facilitating visual inspection and threshold selection. The estimator of Wager (2014) is also asymptotically normal under second-order regular variation with $\rho < 0$. Wager recommends using empirical risk minimization to choose n_u : the procedure is based on a finite-difference approximation of the squared derivative of the process, subject to a penalty term, which corresponds to the expected bias. Although the computational cost is higher than for Hill’s estimator, it can be kept reasonable by restricting n_u .

7 Numerical results

7.1 Simulation study

Assessing the performance of threshold selection methods is hard because there is no right answer, but there are approaches to avoid. For example, data rarely show sharp changes in tail behaviour, so spliced distributions are typically unrealistic as a basis for comparing methods. Moreover, since the tail index ξ is rarely of direct interest, it is unwise to focus on it, particularly on its limiting value, which can provide a poor fit in finite samples (Section B), while the asymptotic bias involving the second-order conditions would be unknown in practice. Risk measures of more practical interest are typically exceedance probabilities or high

quantiles, whose sampling distributions are usually quite skewed (cf. [Belzile and Davison, 2022](#)). Stability of these estimates is crucial, as showcased in [Figure 1](#).

[Section C](#) describes the results of a very extensive simulation study, whose general findings we summarise here. Our study considers a wide range of distributions, and targets their 0.999 quantiles using various sample sizes. A key aspect is the sensitivity of threshold selection procedures to the distribution and sample size, and whether the chosen thresholds depend much, if at all, on the scenario. The threshold selection methods we consider are either parametric (where parameters are estimated via maximum likelihood) or semiparametric (mostly based on Hill’s estimator or variants thereof, coupled with Weissman’s quantile estimator).

In the simulations for the parametric methods, we use a grid \mathcal{U} at equispaced quantile levels, estimated empirically for each dataset to ensure constant numbers of exceedances. We devise an oracle that finds the threshold for which the 0.999 quantile estimator is closest to the true one. This returns thresholds that are usually between the 0.87 and the 0.9 quantiles, suggesting that the variability of the estimators is as important as threshold selection. The performance of the maximum likelihood estimator degrades when $\xi \geq 0.5$, but such tails arise rarely in applications. Unless there are strong penultimate effects, most methods prioritize large samples, and many of the automated procedures return the lowest possible threshold, with the mode for most scenarios being the 0.8 quantile. The selection methods of [Collings et al. \(2025\)](#) and the maximum posterior weight and Bayesian model averaging estimator of [Northrop, Attalides and Jonathan \(2017\)](#) perform reasonably well, though no procedure is uniformly best across all distributions. Rounding and serial correlation have little impact on threshold selection, although autocorrelation leads to large bias in the return level estimates unless accounted for.

Some of the semiparametric threshold selection procedures are promising, but again there is no clear winner. Some procedures yield erratic results, fail to converge, and are very slow. We give advice on which method works best depending on the user case, and list some that should be disregarded altogether. Methods that fix the second-order regular variation parameter tend to be more robust, even if this induces misspecification and bias. Methods that return too small values of n_u lead to overly variable results. Bootstrap estimation of the AMSE via bootstrap is expensive, but works seemingly well. The method of [Guillou and Hall \(2001\)](#) and the SAMSEE estimator of [Schneider, Krajina and Krivobokova \(2021\)](#) are also competitive.

As one would expect, increasing the sample size n leads to both larger n_u and smaller sample fractions kept for inference, i.e., n_u/n decreases with n . The semiparametric methods are quite sensitive to the data passed to them, with many giving results that depend strongly on the choice of candidate thresholds. Restricting threshold selection from the set of order statistics to a range of say $n_u \in [20, 1000]$ can reduce both the variance of quantile estimates and generally the variance for most methods, although it biases shape parameter estimation when $\xi > 0.5$.

7.2 Data application

[Tables 1](#) and [2](#) report results for the application of most of the threshold selection procedures discussed here to the Padova rainfall data; results for four other data sets are in [Section D](#). Although a wide variety of thresholds and thus of shape parameters are selected, the semiparametric estimates of the shape based on Hill’s estimator are generally higher than their maximum likelihood counterparts, but mostly give lower quantile estimates; the shape estimates are largely responsible for these differences, whatever the threshold. Many of the parametric methods return the lowest threshold tested: one could consider lower thresholds, but this would yield a poor fit to the largest observations.

Table 1 Parametric threshold selection for the Padova rainfall data, using candidate thresholds u equispaced on the quantile levels ranging 0.8 to 0.995 in increments of 0.005. The 100-year return levels (in mm) and shape parameters returned are maximum likelihood estimates, except for the Bayesian model averaging of Northrop, Attalides and Jonathan (2017) which gives posterior means based on validation weights at the 0.99 quantile.

method	u	level (%)	n_u	shape	return level
Caers, Beirlant and Maes (1999)	13.80	80.5	645	0.07	108.4
Gonzalo and Olmo (2004)	53.09	99.0	34	0.09	117.4
Thompson et al. (2009)	18.50	86.5	446	0.09	110.6
Sèveges and Davison (2010)	16.00	83.5	544	0.08	109.8
Northrop and Coleman (2014)	53.09	99.0	34	0.09	117.4
Langousis et al. (2016)	13.58	80.0	663	0.08	109.5
Wadsworth (2016)	13.58	80.0	663	0.08	109.5
Northrop, Attalides and Jonathan (2017)			368	0.13	119.0
Silva Lomba and Fraga Alves (2020)	39.97	97.5	83	0.21	122.2
Kiran and Srinivas (2021)	37.93	97.0	100	0.24	124.6
Varty et al. (2021)	13.58	80.0	663	0.08	109.5
Gamet and Jalbert (2022) (beta EGP model)	21.60	89.0	360	0.13	115.2
Murphy, Tawn and Varty (2025)	13.58	80.0	663	0.08	109.5
Collings et al. (2025)	22.49	90.0	332	0.12	114.8

Table 2 Semiparametric threshold selection for the Padova rainfall data. Columns give the selected threshold u , the number of exceedances n_u , the shape parameter based on Hill's estimator (except for Wager (2014)), and the estimated 100-year return levels (in mm) computed using Weissman's estimator.

method	u	n_u	shape	return level
Hall and Welsh (1985)	48.5	41	0.31	139.9
Hall (1990)	33.8	131	0.32	146.7
Beirlant, Vynckier and Teugels (1996a)	13.5	665	0.21	48.0
Drees and Kaufmann (1998)	117.6	1	0.29	107.2
Guillou and Hall (2001)	33.4	138	0.32	144.2
Danielsson et al. (2001)	58.2	28	0.24	118.1
Dupuis and Victoria-Feser (2003) (non-robust)	76.4	10	0.20	113.7
Reiss and Thomas (2007) (l_1)	24.2	297	0.37	180.1
Reiss and Thomas (2007) (l_2)	16.0	548	0.51	347.8
Goegebeur, Beirlant and de Wet (2008)	30.2	179	0.34	159.7
Clauset, Shalizi and Newman (2009)	31.6	167	0.32	146.0
Gomes, Figueiredo and Neves (2012)	48.0	45	0.30	136.1
Gomes et al. (2013) (sample paths)	48.8	39	0.32	143.1
Caeiro and Gomes (2014)	25.4	265	0.37	175.7
Wager (2014)	16.1	541	0.25	69.8
Caeiro and Gomes (2016) (AMSE)	36.0	114	0.31	139.2
Danielsson et al. (2019) (eye-balling)	78.8	7	0.25	118.3
Danielsson et al. (2019) (MAD)	36.8	107	0.30	136.2
Danielsson et al. (2019) (KS)	39.3	88	0.30	134.0
Bladt, Albrecher and Beirlant (2020)	76.6	10	0.20	114.0
Schneider, Krajina and Krivobokova (2021) (SAMSEE)	43.5	62	0.29	131.9

8 Discussion

8.1 Practical considerations

8.1.1 *Multiple hypothesis testing* The starting point is typically a predefined sequence of potential ordered thresholds $\mathcal{U} = \{u_1, \dots, u_J\}$, often high sample quantiles. The highest is chosen to be low enough that estimation based on its exceedances is reliable, and the lowest often lies well inside the dataset. In either case threshold selection is implicitly seen

as equivalent to a sequence of tests of the hypotheses $\mathcal{H}_j : Y - u_j \mid Y > u_j \sim \text{GP}(\sigma_j, \xi)$, for $u_j \in \mathcal{U}$. The threshold-stability of the GPD implies that the hypotheses are nested, i.e., $\mathcal{H}_j \subset \dots \subset \mathcal{H}_1$. If \mathcal{H}_j is true, then \mathcal{H}_l is true for all $l \geq j$, so we seek the smallest k for which \mathcal{H}_k is true. Since $\mathcal{H}_1, \dots, \mathcal{H}_{k-1}$ are then false, it seems natural to deal with the multiple testing using a procedure such as ForwardStop or StrongStop (G'Sell et al., 2016), though these rely on independence of the null p -values. Under this assumption both procedures control the false discovery rate, and StrongStop also controls the family-wise error rate. In threshold selection this error rate is the probability that the selected threshold is too high, and the overall power is related to the probability that it is too low. The procedures described above do not provide independent null p -values, so the proofs of their properties fail.

Since the \mathcal{H}_j specify the models only above the u_j , the samples differ from one model to the next and so likelihood ratio tests or information criteria cannot be applied. It would be possible to use only exceedances above u_j as test samples, though the asymptotics would be non-standard. Extended models such as those described in Section 4.3, which specify the fit over the whole domain or at least above u_1 , are not subject to these restrictions. These models are generally difficult to fit but have the advantage that the threshold is amenable to selection using information criteria.

8.1.2 Many series The number of separate variables or time series for which thresholds must be chosen is large in financial data, in spatial settings, and in other large-scale applications. Such settings require some degree of automation, in particular since individual inspection of graphs for huge numbers of series is precluded. Another aspect, typically ignored, is any dependence between series, which should lead one to select similar thresholds. Smoothing of some sort could improve estimation, and joint tests of adequacy could be constructed, and perhaps used to borrow strength for threshold selection.

8.1.3 Nonstationarity In many cases, the marginal distribution varies over time or depends on covariates. In such cases applied workers often attempt to obtain approximately stationary data by analysing time windows, such as seasons, and analysing these separately.

An alternative is a non-stationary threshold (e.g., Coles, 2001, Chapters 6–7). This can lead to difficulties in obtaining marginal or conditional return levels below the threshold, but there are many such proposals in the literature (e.g., Coelho et al., 2008; Northrop and Jonathan, 2011), including the use of quantile regression using an asymmetric Laplace distribution (Youngman, 2019; Fasiolo et al., 2021) or extremal random forests (Gnecco, Terefe and Engelke, 2024). These methods fix the threshold level relatively low (0.8 or 0.9, say), as such models require appreciable data for reliable estimation.

8.1.4 Ties Much environmental data is recorded with limited accuracy, which prevents use of estimators based on log differences of order statistics. This is awkward in semiparametric settings, but can be handled in a likelihood framework by treating observations as interval-censored; for an example of these impacts and mitigation strategies, see Varty et al. (2021).

8.2 General

Our review highlights the inherent limitations of threshold selection procedures. No approach is entirely satisfactory, but the simulation studies and implementations reveal some overarching features that are worth highlighting.

While asymptotic normality of Hill-type estimators is obtained under an assumption of second-order regular variation, estimates of the second-order parameter ρ are typically far too noisy to be useful: more stable methods are obtained by fixing it to a negative value,

or bypassing its estimation completely, as in Wager (2014). Many algorithms consider all potential choices of threshold, irrespective of the minimum number of exceedances needed for reliable estimation, or of the fact that only the largest observations should be selected.

Parametric methods are generally less easy to automate, and automatic procedures such as that of Langousis et al. (2016) often give unsatisfactory results. We have made pragmatic choices in doing tests sequentially (from the highest selected thresholds) to reflect what seems to be common practice when interpreting threshold stability plots and related procedures. Some of the more promising methods are based on measures of fit and certain apparently *ad hoc* methods (e.g., Thompson et al., 2009) seem to perform well in practice.

Are we barking up the wrong tree? In most cases the transition from the bulk of the distribution to the limiting tail behaviour is gradual, so there is no “correct threshold” to be chosen. This has led to the emergence of sub-asymptotic, extended generalised Pareto models, but it is unclear whether the associated increase in uncertainty for the main quantities of interest is a price worth paying.

Acknowledgements

We thank Sonia Alouini for valuable discussions and for detailed feedback on an earlier draft, and Marco Marani for providing the Padova data. The work was supported by the Swiss National Science Foundation and by the Natural Sciences and Engineering Research Council through grants RGPIN-2022-05001 and DGEER-2022-00461.

Reproducibility

This paper used code from **R** packages `mev` (Belzile, 2026), `tea` (Ossberger, 2020) and `threshr` (Northrop and Attalides, 2026). Code for reproducing the results of this paper is available at <https://github.com/lbelzile/choosing-threshold>.

References

- BADER, B., YAN, J. and ZHANG, X. (2018). Automated threshold selection for extreme value analysis via ordered goodness-of-fit tests with adjustment for false discovery rate. *The Annals of Applied Statistics* **12** 310–329. <https://doi.org/10.1214/17-aos1092>
- BALKEMA, A. A. and DE HAAN, L. (1974). Residual life time at great age. *Annals of Probability* **2** 792–804. <https://doi.org/10.1214/aop/1176996548>
- BEHRENS, C. N., LOPES, H. F. and GAMERMAN, D. (2004). Bayesian analysis of extreme events with threshold estimation. *Statistical Modelling* **4** 227–244. <https://doi.org/10.1191/1471082X04st075oa>
- BEIRLANT, J., DIERCKX, G. and GUILLOU, A. (2005). Estimation of the extreme-value index and generalized quantile plots. *Bernoulli* **11** 949–970.
- BEIRLANT, J., VYNCKIER, P. and TEUGELS, J. L. (1996a). Excess functions and estimation of the extreme-value index. *Bernoulli* **2** 293–318.
- BEIRLANT, J., VYNCKIER, P. and TEUGELS, J. L. (1996b). Tail index estimation, Pareto quantile plots regression diagnostics. *Journal of the American Statistical Association* **91** 1659–1667. <https://doi.org/10.1080/01621459.1996.10476735>
- BEIRLANT, J., DIERCKX, G., GOEGBEUR, Y. and MATTHYS, G. (1999). Tail index estimation and an exponential regression model. *Extremes* **2** 177–200. <https://doi.org/10.1023/a:1009975020370>
- BEIRLANT, J., DIERCKX, G., GUILLOU, A. and STĂRICĂ, C. (2002). On exponential representations of log-spacings of extreme order statistics. *Extremes* **5** 157–180. <https://doi.org/10.1023/a:1022171205129>
- BELZILE, L. R. (2026). `mev`: Modelling of Extreme Values. R package version 2.2. <https://doi.org/10.32614/CRAN.package.mev>
- BELZILE, L. R. and DAVISON, A. C. (2022). Improved inference on risk measures for univariate extremes. *The Annals of Applied Statistics* **16** 1524–1549. <https://doi.org/10.1214/21-aos1555>

- BLADT, M., ALBRECHER, H. and BEIRLANT, J. (2020). Threshold selection and trimming in extremes. *Extremes* **23** 629–665. <https://doi.org/10.1007/s10687-020-00385-0>
- BÜCHER, A. and ZHOU, C. (2021). A horse race between the block maxima method and the peak-over-threshold approach. *Statistical Science* **36** 360–378. <https://doi.org/10.1214/20-sts795>
- BUITENDAG, S., BEIRLANT, J. and DE WET, T. (2020). Confidence intervals for extreme Pareto-type quantiles. *Scandinavian Journal of Statistics* **47** 36–55. <https://doi.org/10.1111/sjos.12396>
- CAEIRO, F. and GOMES, I. (2014). On the bootstrap methodology for the estimation of the tail sample fraction. In *Proceedings of COMPSTAT 2014* 545–552.
- CAEIRO, F. and GOMES, M. I. (2016). Threshold selection in extreme value analysis. In *Extreme Value Modeling and Risk Analysis: Methods and Applications* (D. K. Dey and J. Yan, eds.) 69–86. CRC Press, Boca Raton, FL. <https://doi.org/10.1201/b19721>
- CAERS, J., BEIRLANT, J. and MAES, M. A. (1999). Statistics for modeling heavy tailed distributions in geology: Part I. Methodology. *Mathematical Geology* **31** 391–410. <https://doi.org/10.1023/a:1007538624271>
- CARREAU, J. and BENGIO, Y. (2009). A hybrid Pareto mixture for conditional asymmetric fat-tailed distributions. *IEEE Transactions on Neural Networks* **20** 1087–1101. <https://doi.org/10.1109/tnn.2009.2016339>
- CHOUKAKIAN, V. and STEPHENS, M. A. (2001). Goodness-of-fit tests for the generalized Pareto distribution. *Technometrics* **43** 478–484. <https://doi.org/10.1198/00401700152672573>
- CLAUSET, A., SHALIZI, C. R. and NEWMAN, M. E. J. (2009). Power-law distributions in empirical data. *SIAM Review* **51** 661–703. <https://doi.org/10.1137/070710111>
- COELHO, C. A. S., FERRO, C. A. T., STEPHENSON, D. B. and STEINSKOG, D. J. (2008). Methods for exploring spatial and temporal variability of extreme events in climate data. *Journal of Climate* **21** 2072–2092. <https://doi.org/10.1175/2007jcli1781.1>
- COLES, S. (2001). *An Introduction to Statistical Modeling of Extreme Values*. Springer-Verlag, London. <https://doi.org/10.1007/978-1-4471-3675-0>
- COLLINGS, T. P., MURPHY-BARLTROP, C. J. R., MURPHY, C., HAIGH, I. D., BATES, P. D. and QUINN, N. D. (2025). Automated tail-informed threshold selection for extreme coastal sea levels. *Natural Hazards and Earth System Sciences* **25** 4545–4562. <https://doi.org/10.5194/nhess-25-4545-2025>
- CSÖRGO, S., DEHEUVELS, P. and MASON, D. (1985). Kernel estimates of the tail index of a distribution. *The Annals of Statistics* **13** 1050–1077. <https://doi.org/10.1214/aos/1176349656>
- CURCEAC, S., ATKINSON, P. M., MILNE, A., WU, L. and HARRIS, P. (2020). An evaluation of automated GPD threshold selection methods for hydrological extremes across different scales. *Journal of Hydrology* **585** 124845. <https://doi.org/10.1016/j.jhydrol.2020.124845>
- DANIELSSON, J., DE HAAN, L., PENG, L. and DE VRIES, C. G. (2001). Using a bootstrap method to choose the sample fraction in tail index estimation. *Journal of Multivariate Analysis* **76** 226–248. <https://doi.org/10.1006/jmva.2000.1903>
- DANIELSSON, J., ERGUN, L., DE VRIES, C. G. and DE HAAN, L. (2019). Tail index estimation: quantile-driven threshold selection. <https://doi.org/10.34989/swp-2019-28>
- DAVISON, A. C. (1984). Modelling excesses over high thresholds, with an application. In *Statistical Extremes and Applications*, (J. T. de Oliveira, ed.) *NATO ASI Series* **131** 461–482. Springer Netherlands. https://doi.org/10.1007/978-94-017-3069-3_34
- DAVISON, A. C. and HINKLEY, D. V. (1997). *Bootstrap Methods and Their Application*. Cambridge University Press, Cambridge.
- DAVISON, A. C. and SMITH, R. L. (1990). Models for exceedances over high thresholds (with Discussion). *Journal of the Royal Statistical Society. Series B. (Methodological)* **52** 393–442. <https://doi.org/10.1111/j.2517-6161.1990.tb01796.x>
- DE HAAN, L. and FERREIRA, A. (2006). *Extreme Value Theory: An Introduction*. Springer, New York. <https://doi.org/10.1007/0-387-34471-3>
- DE HAAN, L. and PENG, L. (1998). Comparison of tail index estimators. *Statistica Neerlandica* **52** 60–70. <https://doi.org/10.1111/1467-9574.00068>
- DE HAAN, L. and RESNICK, S. (1996). Second-order regular variation and rates of convergence in extreme-value theory. *The Annals of Probability* **24** 97–124. <https://doi.org/10.1214/aop/1042644709>
- DE ZEA BERMUDEZ, P., AMARAL TURKMAN, M. A. and TURKMAN, K. F. (2001). A predictive approach to tail probability estimation. *Extremes* **4** 295–314. <https://doi.org/10.1023/a:1016546027962>
- DEKKERS, A. L. M. and DE HAAN, L. (1989). On the estimation of the extreme-value index and large quantile estimation. *The Annals of Statistics* **17** 1795–1832. <https://doi.org/10.1214/aos/1176347396>
- DEL CASTILLO, J. and DAOUDI, J. (2009). Estimation of the generalized Pareto distribution. *Statistics & Probability Letters* **79** 684–688. <https://doi.org/10.1016/j.spl.2008.10.021>
- DEL CASTILLO, J. and PADILLA, M. (2016). Modelling extreme values by the residual coefficient of variation. *Statistics and Operations Research Transactions* **40** 303–320. <https://doi.org/10.2436/20.8080.02.45>

- DO NASCIMENTO, F. F., GAMERMAN, D. and LOPES, H. F. (2012). A semiparametric Bayesian approach to extreme value estimation. *Statistics and Computing* **22** 661–675. <https://doi.org/10.1007/s11222-011-9270-z>
- DRAISMA, G., DE HAAN, L., PENG, L. and PEREIRA, T. T. (1999). A bootstrap-based method to achieve optimality in estimating the extreme-value index. *Extremes* **2** 367–404. <https://doi.org/10.1023/a:1009900215680>
- DREES, H., FERREIRA, A. and DE HAAN, L. (2004). On maximum likelihood estimation of the extreme value index. *The Annals of Applied Probability* **14** 1179–1201. <https://doi.org/10.1214/105051604000000279>
- DREES, H. and KAUFMANN, E. (1998). Selecting the optimal sample fraction in univariate extreme value estimation. *Stochastic Processes and their Applications* **75** 149–172. [https://doi.org/10.1016/s0304-4149\(98\)00017-9](https://doi.org/10.1016/s0304-4149(98)00017-9)
- DREES, H., JANSSEN, A., RESNICK, S. I. and WANG, T. (2020). On a minimum distance procedure for threshold selection in tail analysis. *SIAM Journal on Mathematics of Data Science* **2** 75–102. <https://doi.org/10.1137/19m1260463>
- DUPUIS, D. J. (1999). Exceedances over high thresholds: a guide to threshold selection. *Extremes* **1** 251–261. <https://doi.org/10.1023/a:1009914915709>
- DUPUIS, D. J. and VICTORIA-FESER, M.-P. (2003). A prediction error criterion for choosing the lower quantile in Pareto index estimation Technical Report, University of Geneva.
- DUPUIS, D. J. and VICTORIA-FESER, M.-P. (2006). A robust prediction error criterion for Pareto modelling of upper tails. *The Canadian Journal of Statistics* **34** 639–658. <https://doi.org/10.1002/cjs.5550340406>
- FASIOLO, M., WOOD, S. N., ZAFFRAN, M., NEDELLEC, R. and GOUDE, Y. (2021). Fast calibrated additive quantile regression. *Journal of the American Statistical Association* **116** 1402–1412. <https://doi.org/10.1080/01621459.2020.1725521>
- FERRO, C. A. T. and SEGERS, J. (2003). Inference for clusters of extreme values. *Journal of the Royal Statistical Society: Series B (Statistical Methodology)* **65** 545–556. <https://doi.org/10.1111/1467-9868.00401>
- FEUERVERGER, A. and HALL, P. (1999). Estimating a tail exponent by modelling departure from a Pareto distribution. *The Annals of Statistics* **27** 760–781. <https://doi.org/10.1214/aos/1018031215>
- FISHER, R. A. and TIPPETT, L. H. C. (1928). Limiting forms of the frequency distributions of the largest or smallest member of a sample. *Mathematical Proceedings of the Cambridge Philosophical Society* **24** 180–190.
- FRIGESSI, A., HAUG, O. and RUE, H. (2002). A dynamic mixture model for unsupervised tail estimation without threshold selection. *Extremes* **5** 219–235. <https://doi.org/10.1023/a:1024072610684>
- FUKUTOME, S., LINIGER, M. A. and SÜVEGES, M. (2015). Automatic threshold and run parameter selection: a climatology for extreme hourly precipitation in Switzerland. *Theoretical and Applied Climatology* **120** 403–416. <https://doi.org/10.1007/s00704-014-1180-5>
- GAMET, P. and JALBERT, J. (2022). A flexible extended generalized Pareto distribution for tail estimation. *Environmetrics* **33**. <https://doi.org/10.1002/env.2744>
- GNECCO, N., TEREFE, E. M. and ENGELKE, S. (2024). Extremal random forests. *Journal of the American Statistical Association* **119** 3059–3072. <https://doi.org/10.1080/01621459.2023.2300522>
- GNEDENKO, B. V. (1943). Sur la distribution limite du terme maximum d’une série aléatoire. *Annals of Mathematics* **44** 423–453. <https://doi.org/10.2307/1968974>
- GOEGBEUR, Y., BEIRLANT, J. and DE WET, T. (2008). Linking Pareto-tail kernel goodness-of-fit statistics with tail index at optimal threshold and second order estimation. *REVSTAT-Statistical Journal* **6** 51–69. <https://doi.org/10.57805/revstat.v6i1.57>
- GOMES, M. I., FIGUEIREDO, F. and NEVES, M. M. (2012). Adaptive estimation of heavy right tails: resampling-based methods in action. *Extremes* **15** 463–489. <https://doi.org/10.1007/s10687-011-0146-6>
- GOMES, M. I. and OLIVEIRA, O. (2001). The bootstrap methodology in statistics of extremes—choice of the optimal sample fraction. *Extremes* **4** 331–358. <https://doi.org/10.1023/a:1016592028871>
- GOMES, M. I., HENRIQUES-RODRIGUES, L., ALVES, M. I. F. and MANJUNATH, B. G. (2013). Adaptive PORT–MVRB estimation: an empirical comparison of two heuristic algorithms. *Journal of Statistical Computation and Simulation* **83** 1129–1144. <https://doi.org/10.1080/00949655.2011.652113>
- GONZALO, J. and OLMO, J. (2004). Which extreme values are really extreme? *Journal of Financial Econometrics* **2** 349–369. <https://doi.org/10.1093/jjfinec/nbh014>
- GRIMSHAW, S. D. (1993). Computing maximum likelihood estimates for the generalized Pareto distribution. *Technometrics* **35** 185–191. <https://doi.org/10.1080/00401706.1993.10485040>
- G’SELL, M. G., WAGER, S., CHOULDECHOVA, A. and TIBSHIRANI, R. (2016). Sequential selection procedures and false discovery rate control. *Journal of the Royal Statistical Society: Series B (Statistical Methodology)* **78** 423–444. <https://doi.org/10.1111/rssb.12122>
- GUILLOU, A. and HALL, P. (2001). A diagnostic for selecting the threshold in extreme value analysis. *Journal of the Royal Statistical Society: Series B (Statistical Methodology)* **63** 293–305. <https://doi.org/10.1111/1467-9868.00286>

- GUMBEL, E. J. (1958). *Statistics of Extremes*. Columbia University Press, New York. <https://doi.org/10.7312/gumb92958>
- HALL, P. (1990). Using the bootstrap to estimate mean squared error and select smoothing parameter in nonparametric problems. *Journal of Multivariate Analysis* **32** 177–203. [https://doi.org/10.1016/0047-259x\(90\)90080-2](https://doi.org/10.1016/0047-259x(90)90080-2)
- HALL, P. and WELSH, A. H. (1985). Adaptive estimates of parameters of regular variation. *The Annals of Statistics* **13** 331–341. <https://doi.org/10.1214/aos/1176346596>
- HILL, B. M. (1975). A simple general approach to inference about the tail of a distribution. *Annals of Statistics* **3** 1163–1174. <https://doi.org/10.1214/aos/1176343247>
- HOSKING, J. R. M. (1990). *L*-moments: Analysis and estimation of distributions using linear combinations of order statistics. *Journal of the Royal Statistical Society: Series B (Methodological)* **52** 105–124. <https://doi.org/10.1111/j.2517-6161.1990.tb01775.x>
- HOSKING, J. R. M. and WALLIS, J. R. (1987). Parameter and quantile estimation for the generalized Pareto distribution. *Technometrics* **29** 339–349. <https://doi.org/10.1080/00401706.1987.10488243>
- HU, Y. and SCARROTT, C. (2018). *evmix*: An R package for extreme value mixture modeling, threshold estimation and boundary corrected kernel density estimation. *Journal of Statistical Software* **84** 1–27. <https://doi.org/10.18637/jss.v084.i05>
- HUET, N., NAVEAU, P. and SABOURIN, A. (2026). Multi-site modelling and reconstruction of past extreme skew surges along the French Atlantic coast. *Journal of the Royal Statistical Society Series C: Applied Statistics* [qlag024](https://doi.org/10.1093/jrssc/qlag024). <https://doi.org/10.1093/jrssc/qlag024>
- KIRAN, K. G. and SRINIVAS, V. V. (2021). A Mahalanobis distance-based automatic threshold selection method for peaks over threshold model. *Water Resources Research* **57**. <https://doi.org/10.1029/2020wr027534>
- LANGOUSIS, A., MAMALAKIS, A., PULIGA, M. and DEIDDA, R. (2016). Threshold detection for the generalized Pareto distribution: Review of representative methods and application to the NOAA NCDC daily rainfall database. *Water Resources Research* **52** 2659–2681. <https://doi.org/10.1002/2015WR018502>
- LEE, J., FAN, Y. and SISSON, S. A. (2015). Bayesian threshold selection for extremal models using measures of surprise. *Computational Statistics & Data Analysis* **85** 84–99. <https://doi.org/10.1016/j.csda.2014.12.004>
- MACDONALD, A. E. (2011). Extreme value mixture modelling with medical and industrial applications, PhD thesis, University of Canterbury. <https://doi.org/10.26021/1970>
- MACDONALD, A. E., SCARROTT, C. J., LEE, D., DARLOW, B., REALE, M. and RUSSELL, G. (2011). A flexible extreme value mixture model. *Computational Statistics & Data Analysis* **55** 2137–2157. <https://doi.org/10.1016/j.csda.2011.01.005>
- MARANI, M. and ZANETTI, S. (2015). Long-term oscillations in rainfall extremes in a 268 year daily time series. *Water Resources Research* **51** 639–647. <https://doi.org/10.1002/2014wr015885>
- MASON, D. M. and TUROVA, T. S. (1994). *Weak convergence of the Hill estimator process* In *Extreme Value Theory and Applications: Proceedings of the Conference on Extreme Value Theory and Applications* 419–431. Springer, Boston, MA. https://doi.org/10.1007/978-1-4613-3638-9_25
- MÍNGUEZ, R. (2025). Automatic threshold selection for generalized Pareto and Pareto–Poisson distributions in rainfall analysis: A case study using the NOAA NCDC daily rainfall database. *Atmosphere* **16**. <https://doi.org/10.3390/atmos16010061>
- MURPHY, C., TAWN, J. A. and VARTY, Z. (2025). Automated threshold selection and associated inference uncertainty for univariate extremes. *Technometrics* **67** 215–224. <https://doi.org/10.1080/00401706.2024.2421744>
- NAVEAU, P. (2025). Jointly modeling bulk and tails. In *Handbook of Statistics of Extremes* (M. de Carvalho, R. Huser, P. Naveau, and B. J. Reich, eds.) to appear. Chapman & Hall/CRC, Boca Raton.
- NAVEAU, P., HUSER, R., RIBEREAU, P. and HANNART, A. (2016). Modeling jointly low, moderate, and heavy rainfall intensities without a threshold selection. *Water Resources Research* **52** 2753–2769. <https://doi.org/10.1002/2015WR018552>
- NEVES, C. and FRAGA ALVES, M. I. (2004). Reiss and Thomas’ automatic selection of the number of extremes. *Computational Statistics & Data Analysis* **47** 689–704. <https://doi.org/10.1016/j.csda.2003.11.011>
- NORTHROP, P. J., ATTALIDES, N. and JONATHAN, P. (2017). Cross-validatory extreme value threshold selection and uncertainty with application to ocean storm severity. *Journal of the Royal Statistical Society: Series C (Applied Statistics)* **66** 93–120. <https://doi.org/10.1111/rssc.12159>
- NORTHROP, P. J. and ATTALIDES, N. (2026). *threshr*: Threshold Selection and Uncertainty for Extreme Value Analysis R package version 1.0.8. <https://doi.org/10.32614/CRAN.package.threshr>
- NORTHROP, P. J. and COLEMAN, C. L. (2014). Improved threshold diagnostic plots for extreme value analyses. *Extremes* **17** 289–303. <https://doi.org/10.1007/s10687-014-0183-z>
- NORTHROP, P. J. and JONATHAN, P. (2011). Threshold modelling of spatially dependent non-stationary extremes with application to hurricane-induced wave heights. *Environmetrics* **22** 799–809. <https://doi.org/10.1002/env.1106>

- OORSCHOT, J., SEGERS, J. and ZHOU, C. (2023). Tail inference using extreme U -statistics. *Electronic Journal of Statistics* **17** 1113–1159. <https://doi.org/10.1214/23-ejs2129>
- OSSBERGER, J. (2020). `tea`: Threshold Estimation Approaches. R package version 1.1. <https://doi.org/10.32614/CRAN.package.tea>
- PAPASTATHOPOULOS, I. and TAWN, J. A. (2013). Extended generalised Pareto models for tail estimation. *Journal of Statistical Planning and Inference* **143** 131–143. <https://doi.org/10.1016/j.jspi.2012.07.001>
- PICKANDS, J. (1975). Statistical inference using extreme order statistics. *The Annals of Statistics* **3** 119–131. <https://doi.org/10.1214/aos/1176343003>
- REISS, R. D. and THOMAS, M. (2007). *Statistical Analysis of Extreme Values: with Applications to Insurance, Finance, Hydrology and Other Fields*. Springer Birkhäuser. <https://doi.org/10.1007/978-3-7643-7399-3>
- RÉNYI, A. (1953). On the theory of order statistics. *Acta Mathematica Academiae Scientiarum Hungarica* **4** 191–231. <https://doi.org/10.1007/BF02127580>
- RESNICK, S. I. (2006). *Heavy-Tail Phenomena: Probabilistic and Statistical Modeling*. Springer, New York. <https://doi.org/10.1007/978-0-387-45024-7>
- RIVERA MANCIA, M. E. (2014). Modelling operational risk using a Bayesian approach to extreme value theory, PhD thesis, McGill University. <https://doi.org/10.82308/23628>
- SCARROTT, C. J. and MACDONALD, A. E. (2012). A review of extreme-value threshold estimation and uncertainty quantification. *REVSTAT – Statistical Journal* **10** 33–60. <https://doi.org/10.57805/revstat.v10i1.110>
- SCHNEIDER, L. F., KRAJINA, A. and KRIVOBOKOVA, T. (2021). Threshold selection in univariate extreme value analysis. *Extremes* **24** 881–913. <https://doi.org/10.1007/s10687-021-00405-7>
- SILVA LOMBA, J. and FRAGA ALVES, M. I. (2020). L -moments for automatic threshold selection in extreme value analysis. *Stochastic Environmental Research and Risk Assessment* **34** 465–491. <https://doi.org/10.1007/s00477-020-01789-x>
- SINCLAIR, C. D., SPURR, B. D. and AHMAD, M. I. (1990). Modified Anderson Darling test. *Communications in Statistics — Theory and Methods* **19** 3677–3686. <https://doi.org/10.1080/03610929008830405>
- SMITH, R. L. (1984). Threshold methods for sample extremes. In *Statistical Extremes and Applications* (J. T. de Oliveira, ed.) 621–638. Reidel, Dordrecht.
- SMITH, R. L. (1985). Maximum likelihood estimation in a class of nonregular cases. *Biometrika* **72** 67–92. <https://doi.org/10.1093/biomet/72.1.67>
- SMITH, R. L. (1987). Approximations in extreme value theory. Technical Report, Department of Statistics and Operations Research, University of North Carolina.
- SOLARI, S., EGÜEN, M., POLO, M. J. and LOSADA, M. A. (2017). Peaks over threshold (POT): A methodology for automatic threshold estimation using goodness of fit p -value. *Water Resources Research* **53** 2833–2849. <https://doi.org/10.1002/2016wr019426>
- STEIN, M. L. (2021). A parametric model for distributions with flexible behavior in both tails. *Environmetrics* **32** e2658. <https://doi.org/10.1002/env.2658>
- STEIN, M. L. (2023). A weighted composite log-likelihood approach to parametric estimation of the extreme quantiles of a distribution. *Extremes* **26** 469–507. <https://doi.org/10.1007/s10687-023-00466-w>
- SÜVEGES, M. and DAVISON, A. C. (2010). Model misspecification in peaks over threshold analysis. *Ann. Appl. Stat.* **4** 203–221. <https://doi.org/10.1214/09-aos292>
- TANCREDI, A., ANDERSON, C. and O’HAGAN, A. (2006). Accounting for threshold uncertainty in extreme value estimation. *Extremes* **9** 87–106. <https://doi.org/10.1007/s10687-006-0009-8>
- THOMPSON, P., CAI, Y., REEVE, D. and STANDER, J. (2009). Automated threshold selection methods for extreme wave analysis. *Coastal Engineering* **56** 1013–1021. <https://doi.org/10.1016/j.coastaleng.2009.06.003>
- TODOROVIC, P. and ROUSSELLE, J. (1971). Some problems of flood analysis. *Water Resources Research* **7** 1144–1150. <https://doi.org/10.1029/WR007i005p01144>
- TODOROVIC, P. and ZELENHASIC, E. (1970). A stochastic model for flood analysis. *Water Resources Research* **6** 1641–1648. <https://doi.org/10.1029/WR006i006p01641>
- VARTY, Z., TAWN, J. A., ATKINSON, P. M. and BIERMAN, S. (2021). Inference for extreme earthquake magnitudes accounting for a time-varying measurement process. <https://doi.org/10.48550/arXiv.2102.00884>
- VENTURA, V. (2002). Non-parametric bootstrap recycling. *Statistics and Computing* **12** 261–273. <https://doi.org/10.1023/a:1020754911317>
- WADSWORTH, J. L. (2016). Exploiting structure of maximum likelihood estimators for extreme value threshold selection. *Technometrics* **58** 116–126. <https://doi.org/10.1080/00401706.2014.998345>
- WADSWORTH, J. L., TAWN, J. A. and JONATHAN, P. (2010). Accounting for choice of measurement scale in extreme value modeling. *The Annals of Applied Statistics* **4** 1558–1578. <https://doi.org/10.1214/10-aos333>
- WADSWORTH, J. L. and TAWN, J. A. (2012). Likelihood-based procedures for threshold diagnostics and uncertainty in extreme value modelling. *Journal of the Royal Statistical Society: Series B (Statistical Methodology)* **74** 543–567. <https://doi.org/10.1111/j.1467-9868.2011.01017.x>

- WAGER, S. (2014). Subsampling extremes: From block maxima to smooth tail estimation. *Journal of Multivariate Analysis* **130** 335–353. <https://doi.org/10.1016/j.jmva.2014.06.010>
- WEISSMAN, I. (1978). Estimation of parameters and large quantiles based on the k largest observations. *Journal of the American Statistical Association* **73** 812–815. <https://doi.org/10.1080/01621459.1978.10480104>
- WHITE, H. (1982). Maximum likelihood estimation of misspecified models. *Econometrica* **50** 1–25. <https://doi.org/10.2307/1912526>
- YOUNGMAN, B. D. (2019). Generalized additive models for exceedances of high thresholds with an application to return level estimation for U.S. wind gusts. *Journal of the American Statistical Association* **114** 1865–1879. <https://doi.org/10.1080/01621459.2018.1529596>

Appendix A: Exploratory analysis of the Padova data

Figure 6 shows the seasonal and temporal trends for the Padova data. Quantile regression indicates some residual seasonality and nonstationarity; in particular there is a small but statistically significant increase of around 3.4 mm in the 90% quantile from 1950 onwards, but this is smaller than the seasonal variability for the period.

Appendix B: Penultimate approximation

Section 2.1.1 gives a brief account of the theoretical conditions under which the GPD provides a limiting distribution for exceedances over high thresholds, and mentions that under more restrictive but nevertheless reasonable conditions, the GPD also provides a penultimate approximation, albeit with a shape parameter that does not equal its limiting value. Such results are useful, but it is important to appreciate that empirical fitting can improve on both the limiting and penultimate approximations. We illustrate this by maximum likelihood fitting of the GPD to samples of $N = 10^7$ Gaussian observations lying above the $q = 0.9, 0.95$ and 0.99 quantiles, u_q , say, of the Gaussian distribution. The idea is not to reproduce sample sizes that might be met in practice, but to assess how closely the generalized Pareto model can match the ‘true’ truncated Gaussian distribution. The quality of the resulting approximation depends on N ; in principle the fitted shape parameter ξ_N must tend to zero as $N \rightarrow \infty$, but in practice the tail of the truncated distribution is so short that ξ_N is appreciably negative even with this huge value of N .

Figure 7 shows how well the quantiles of the left-truncated Gaussian distributions are matched by those of the limiting exponential distribution, the penultimate approximation with shape parameter ξ_t , and the generalized Pareto distribution fitted by maximum likelihood estimation based on the N exceedances. Although negative, the fitted shape parameters ξ_N are appreciably closer to zero than the penultimate values, and the corresponding quantiles track the true quantiles remarkably well for tail probabilities down to 10^{-4} or so. Maximum likelihood estimators based on samples of size $n_{u_q} \ll N$ would be expected to have means roughly ξ_N , rather than the limiting or penultimate values of ξ , with $O(n_{u_q}^{-1})$ bias.

Similar computations (large-sample maximum likelihood estimates and penultimate approximations) for the shape parameter of a series of distributions (cf. Section C.1) considered

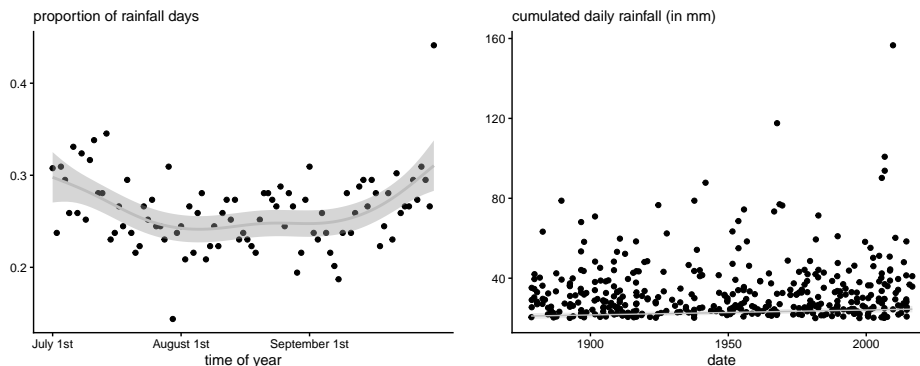


Figure 6 Analysis of seasonality for the Padova data, using only the period for July–September. The left panel shows the proportion of rainy days as a function of the day of the year, with a generalized additive model smooth. The right panel shows the exceedances above 20mm of rainfall, and the estimated quantile regression curve with pointwise Wald 95% confidence intervals, for the 90% of non-zero rainfall.

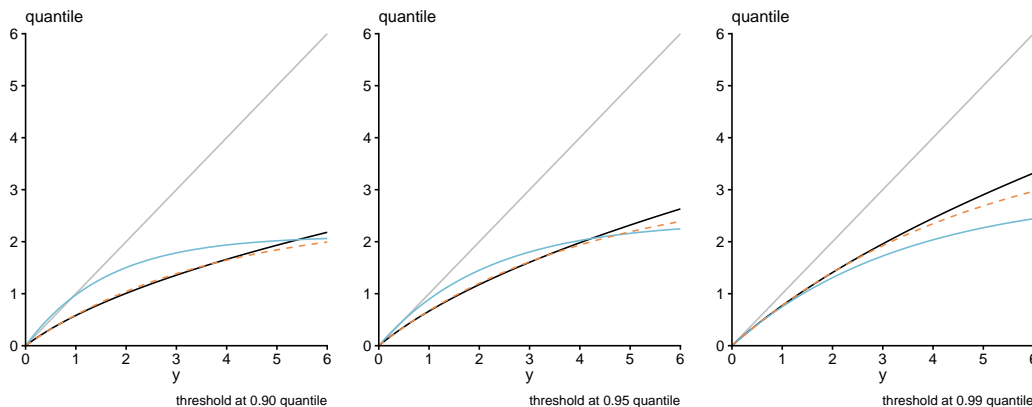


Figure 7 Penultimate fits for ten million exceedances for the Gaussian model with thresholds at its 0.9, 0.95 and 0.99 quantiles (left to right). The limiting distribution is scaled so that the exceedance probability for y is 10^{-y} . The panels show scaled excess quantile plots for the true truncated normal (black), penultimate approximation (full blue), best fitted generalized Pareto (dashed orange) and limiting exponential (grey straight line with unit slope). Curves below the diagonal correspond to the implied excess quantiles from generalized Pareto or the true model. The fitted shape parameters $\hat{\xi}$ are -0.123 , -0.117 and -0.088 , while the penultimate values ξ_t are -0.270 , -0.203 and -0.127 .

in the simulation study are reported in Table 3. They show the same phenomenon, namely that the maximum likelihood values are closer to the limit than are the penultimate values.

Appendix C: Simulation study

In this section we present results from an extensive simulation study that covers some scenarios encountered in applications, including data recorded with limited precision (rounding), and dependent time series with clusters. The data are simulated from a variety of parametric models with different shape parameters and rates of convergence to the limiting model.

We consider return levels for quantile level $q = 0.999$, as this could be reasonably inferred from the data while being extreme enough that empirical estimation is infeasible or too noisy to be useful. As some of the distributions considered have infinite first or second moments, or very different scales, we consider relative errors.

We compare performance in terms of bias and variance (through sampling distribution and absolute bias measures), all relative to the true value. When relevant, we also report the computing time. We also assess the variability of the proportion of exceedances retained or the number of order statistics above u kept by the selection procedure. Some methods may fail to return a threshold, and the percentage of such failures impacts both their practical usefulness and the ease with which they can be studied by simulation.

C.1 Target distributions

Simulation studies should take distributions whose tail behaviour is also plausible in applications — for example, heavy-tailed cases with $\xi \approx 1$ are unrealistic outside of specific financial or network applications, whereas most environmental phenomena (e.g., temperature, wind speed, rainfall) would have reasonable values of $\xi \in [-0.5, 0.25]$ in practice. Many papers on threshold selection have used mixture models: for example, Lee, Fan and Sisson (2015) considered non-overlapping distributions with a generalized Pareto tail above u , and another distribution, right-truncated at u , for the bulk. Such models have a sharp discontinuity at the

threshold u , a feature which simplifies threshold selection but is seldom observed in practice. We therefore instead consider distributions featured in simulation studies of [Choulakian and Stephens \(2001\)](#) (a–d), [Schneider, Krajina and Krivobokova \(2021\)](#) (i–m), and extended generalized Pareto models with exact generalized Pareto limits (e, n–p). Here is our full list:

- | | |
|--|--|
| (a) gamma with shape 2 and scale 1; | (l) loggamma with density function $\log(x)x^{-2}$ for $x \geq 1$ ($\xi = 1$); |
| (b) standard lognormal; | (m) Burr with survival function $(1 + x^2)^{-1}$ for $x > 0$ ($\xi = 0.5$); |
| (c) Weibull with scale 1 and shape 0.75; | (n) piecewise generalized Pareto (Northrop and Coleman, 2014) with shape -0.5 up to the 0.9 quantile and 0.25 above; |
| (d) Weibull with scale 1 and shape 1.25; | (o) third extended generalized Pareto model of Papastathopoulos and Tawn (2013) (power model) with $\xi = -0.2$, unit scale and $\kappa = 0.25$; |
| (e) piecewise generalized Pareto (Northrop and Coleman, 2014) with shape 0.25 up to $u = 1.25$ and -0.25 above | (p) exponential tilting extended generalized Pareto model with shape $\xi = 0.2$ and $\kappa = 0.1$. |
| (f) standard exponential ($\xi = 0$) | |
| (g) generalized Pareto with shape $\xi = 0.15$ | |
| (h) generalized Pareto with shape $\xi = -0.15$ | |
| (i) folded Student- t with 6 degrees of freedom $ T_6 $ ($\xi = 1/6$); | |
| (j) standard Fréchet with shape $\xi = 0.5$; | |
| (k) standard Cauchy ($\xi = 1$) truncated on \mathbb{R}^+ ; | |

The distributions (f–h) are threshold-stable, while the penultimate models (n–p) converge rather slowly to the generalized Pareto limit. Table 3 shows that the average maximum likelihood estimates for the shape for varying quantile levels vary very little, and can differ markedly from the limiting shape value and the penultimate approximation, though the latter tends to be closer to the best fitting model given by the MLE. The fact that the latter barely changes suggests that methods ought to take lowest threshold in most cases, though this does not take into account goodness-of-fit considerations, and small-sample bias is more acute when using higher thresholds. Table 4 shows that, unless convergence to the limit is quite slow (cf. distribution l), the approximation for the 0.999 quantile is quite accurate, that the penultimate approximation can be markedly better than using the limit shape, but that the penultimate approximation is not a panacea, especially at quantiles 0.8 and 0.9.

C.2 Simulation 1

We consider datasets of sizes $n = 2000$, and use a random grid of candidate thresholds \mathcal{U} at the empirical $\{0.8, 0.81, \dots, 0.98\}$ quantiles, thus giving 20 observations between each threshold. We compare the following threshold selection methods:

- P₁. the threshold stability plot of [Davison and Smith \(1990\)](#), using the smallest threshold for which point estimates for the shape are included in the profile-likelihood 95% confidence interval for all higher thresholds;
- P₂. minimization of the mean squared error of the shape parameter by semiparametric bootstrap of [Caers, Beirlant and Maes \(1999\)](#);
- P₃. [Gonzalo and Olmo \(2004\)](#) with absolute distance, mimicking [Pickands \(1975\)](#);
- P₄. [Gonzalo and Olmo \(2004\)](#) with the Kolmogorov–Smirnov statistic;
- P₅. normality tests for coefficients of [Thompson et al. \(2009\)](#) (★);
- P₆. the [Süveges and Davison \(2010\)](#) information matrix test with gap $K = 1$ (★);
- P₇. the score test of [Northrop and Coleman \(2014\)](#) comparing the piecewise generalized Pareto and generalized Pareto models (★);

Table 3 Shape parameters for varying quantile levels (0.8, 0.9, 0.95, 0.99) obtained using *Smith (1987)* penultimate approximation, maximum likelihood estimation with samples of IM exceedances, and the limiting value of ξ for models without exact generalized Pareto tails.

model	penultimate				mle				limit
	80%	90%	95%	99%	80%	90%	95%	99%	
a	-0.11	-0.07	-0.04	-0.02	-0.04	-0.03	-0.02	-0.01	0
b	0.32	0.3	0.28	0.25	0.28	0.26	0.25	0.22	0
c	0.21	0.14	0.11	0.07	0.11	0.09	0.07	0.05	0
d	-0.12	-0.09	-0.07	-0.04	-0.06	-0.05	-0.04	-0.03	0
i	-0.08	0	0.05	0.11	0.06	0.09	0.11	0.14	0.17
j	0.43	0.47	0.49	0.5	0.48	0.49	0.5	0.5	0.5
k	0.93	0.98	1	1	0.99	1	1	1	1
l	1.22	1.19	1.17	1.13	1.17	1.15	1.13	1.11	1
m	0.38	0.44	0.47	0.49	0.47	0.48	0.49	0.5	0.5
o	0.31	0.01	-0.1	-0.18	-0.1	-0.15	-0.18	-0.2	-0.25
p	0.39	0.36	0.31	0.23	0.3	0.27	0.24	0.21	0.2

Table 4 Ratio of estimated 0.999 quantile to the true quantile (in %) for varying quantile levels (0.8, 0.9, 0.95, 0.99) obtained using *Smith (1987)* penultimate approximation, maximum likelihood estimation with samples of IM exceedances, and the limiting value of ξ .

model	penultimate				mle				limit			
	80%	90%	95%	99%	80%	90%	95%	99%	80%	90%	95%	99%
a	90.2	96.2	98.5	99.9	99.5	99.9	100	100	109	104.8	102.7	100.6
b	113.9	109.2	105.2	100.9	102.8	101	100.1	99.7	50.5	59.4	68.3	86.8
c	128.8	110.7	104.4	100.5	102.2	100.5	99.9	99.9	77.3	84.7	90	97.1
d	91.3	96.3	98.4	99.8	99.5	100	100.1	100.1	113.3	108	104.8	101.2
i	77.9	88.8	94.7	99.4	97.8	99.5	100.1	100.2	129.6	116.5	109.2	102
j	83.3	94.2	98	99.9	97.9	99.4	99.9	100	105.3	102.2	101	100.1
k	77.9	95	99	100	97.4	99.5	100	100.1	103.3	100.8	100.2	100
l	138.4	121.5	111.7	102.1	111.2	105	102	99.5	52	59.9	67.7	84.8
m	72.7	89.5	96.2	99.8	96.3	98.9	99.7	100.1	110.3	104.4	101.9	100.2
o	261.9	125.7	106.4	100.3	102.8	100.2	99.8	100	69.8	84.8	92	98.2
p	137.1	124.6	112.4	101	107.1	102.4	100.4	99.9	76.6	85.1	91.8	98.8

- P₈. the mean residual life plot using the automated procedure of [Langousis et al. \(2016\)](#), returning the threshold that minimizes the weighted mean squared error;
- P₉. the [Wadsworth \(2016\)](#) white noise test, returning the smallest threshold at which the white noise hypothesis cannot be rejected based on a change-point likelihood ratio test;
- P₁₀. the posterior predictive model of [Northrop, Attalides and Jonathan \(2017\)](#), returning the threshold with the largest posterior weight;
- P₁₁. [Northrop, Attalides and Jonathan \(2017\)](#), with Bayesian model averaging;
- P₁₂. goodness-of-fit statistics from [Bader, Yan and Zhang \(2018\)](#) (★);
- P₁₃. the [Silva Lomba and Fraga Alves \(2020\)](#) L -moment skewness-kurtosis procedure;
- P₁₄. [Kiran and Srinivas \(2021\)](#) Mahalanobis-distance minimization with L -moments;
- P₁₅. metric-based adjustments of [Varty et al. \(2021\)](#) with exponential quantile-quantile plots with weighted mean squared error;

- P₁₆. the likelihood ratio test to compare the extended generalized Pareto beta model of [Gamet and Jalbert \(2022\)](#) with the generalized Pareto (\star);
- P₁₇. metric-based adjustments of [Murphy, Tawn and Varty \(2025\)](#) with generalized Pareto quantile-quantile plots;
- P₁₈. the [Collings et al. \(2025\)](#) TAILS method.

All tests are performed at the nominal 5% significance level. Procedures marked with a star (\star) return a sequence of p -values for the ordered thresholds, to which a sequential testing procedure such as ForwardStop ([G'Sell et al., 2016](#)) might be applied. By design this systematically leads to the selection of lower thresholds.

We use empirical quantiles from simulated datasets to ensure the number of exceedances stays the same, rather than fixing the thresholds to the true quantiles of the distribution. The latter would facilitate comparisons, but could not be applied in practice.

We also devise an oracle that minimizes the absolute bias among all candidate thresholds; only maximum likelihood estimates evaluated at empirical quantiles in the range $\{0.8, 0.81, \dots, 0.98\}$ are considered; the loss is estimated using a Monte Carlo average with 1000 samples from each scenario, excluding missing values due to failed convergence, or when methods do not return a threshold.

We also checked the effect of varying the sample size, taking $n \in \{1000, 2000, 3000, 4000\}$ and retaining the same quantile level as candidate thresholds, adding the 0.99 quantile for the two largest values of n . We also considered scenarios with serial dependence and rounding. For the first, time series were drawn from a Gaussian autoregressive process of order 1 with correlation coefficient 0.5, and transformed to have the marginal distribution of interest using the probability integral transform. For the rounding, we multiplied each series by a factor equal to one hundred divided by the 0.9 quantile of the distribution, $c = 100/F^{-1}(0.9)$, rounded observations up to the nearest integer to avoid creating zeros, then back-transformed them, viz. $x \mapsto c \lceil x/c \rceil$. This leads to more rounding at lower quantile levels than higher ones.

Summary of results for Simulation 1

Given the number of distributions and methods considered, it is difficult to summarize results. We consider first in [Figure 8](#) the proportion of time a quantile level is returned as threshold (as a function of rounding and truncation), as this is indicative of the sensibility of the method to the underlying data generating process and reveals some methods for which universally, the lowest candidate threshold seems to be favored.

Summary statistics of the sampling distribution of the estimated bias of the 0.999 quantile (relative to the true 0.999 quantile), $(\hat{q}_{0.999} - q_0)/q_0$ are shown in [Figure 10](#). A lot of the performance has to do with the maximum likelihood estimator, and many distributions have similar performances because the threshold selection methods return the same (low) threshold levels; see [Figure 8](#). The median ration of these absolute biases, relative to the oracle, are reported in [Table 5](#).

Increasing the sample size had little effect on choice: most methods display changes of the order 1–2%, so are globally insensitive to sample size. The methods most affected were P₄, P₆ and P₁₃, which saw an increase in the proportion of higher thresholds retained. Method P₈ displayed the reverse tendency, suggesting that the weighting scheme is wholly inadequate. Methods P₅ and P₇, on the other hand, are sensitive to the choice of alternatives and the number of thresholds.

In all cases, ignoring the serial dependence leads to large positive relative biases of the maximum likelihood estimators of quantiles or return levels. Truncation, however, has little to no impact. The information matrix test of P₆, designed for joint estimation of the threshold and extremal index, shows a noticeable increase in the proportion of lowest thresholds

Table 5 Median ratio of absolute difference to the true quantile versus oracle $|q_{method} - q_0|/|q_{oracle} - q_0|$ for different estimation methods (rows) and different distributions (columns) for the estimation of 0.999 quantile for Simulation 1. Smaller numbers are preferable

	a	b	c	d	e	f	g	h	i	j	k	l	m	n	o	p
P ₁	1.6	2.3	2.4	1.5	1.4	1.7	2.0	1.5	1.8	2.8	3.1	3.6	2.4	4.0	2.7	3.4
P ₂	1.5	2.4	2.3	1.5	1.3	1.7	2.0	1.4	1.7	2.6	3.1	3.9	2.3	4.0	2.6	3.2
P ₃	1.7	2.7	2.6	1.6	1.4	1.9	2.1	1.5	1.9	3.0	3.5	4.7	2.6	3.8	2.5	3.4
P ₄	1.9	2.8	2.7	1.7	1.4	2.0	2.4	1.6	2.2	3.6	4.8	5.0	3.2	4.0	2.5	3.5
P ₅	1.6	2.6	2.6	1.6	1.4	1.9	2.2	1.5	1.9	3.1	3.8	4.7	2.6	3.8	2.6	3.4
P ₆	1.7	2.6	2.4	1.6	1.4	1.8	2.2	1.5	1.9	3.1	3.7	4.1	2.6	4.0	2.4	3.2
P ₇	1.9	2.8	2.5	1.8	1.4	1.9	2.5	1.6	2.1	3.6	4.6	5.4	3.4	4.2	2.4	3.5
P ₈	1.5	2.2	2.2	1.5	1.3	1.6	2.0	1.4	1.8	2.6	2.9	3.6	2.3	3.8	2.7	3.3
P ₉	1.7	2.4	2.5	1.6	1.4	1.7	2.1	1.6	1.9	2.7	3.0	3.8	2.4	3.8	2.4	3.4
P ₁₀	1.5	2.3	1.9	1.5	1.3	1.6	1.9	1.3	1.7	2.7	3.1	3.5	2.5	4.1	1.7	2.6
P ₁₁	1.8	2.7	2.5	1.7	1.4	2.0	2.5	1.6	2.2	3.4	4.4	4.6	3.0	4.1	2.6	3.4
P ₁₂	1.8	2.8	2.6	1.7	1.5	2.0	2.3	1.6	2.1	3.3	4.1	4.5	3.0	3.9	2.6	3.4
P ₁₃	1.7	2.5	2.4	1.6	1.3	1.7	2.1	1.5	2.0	2.9	3.5	4.4	2.7	3.8	2.6	3.4
P ₁₄	1.9	3.2	2.8	1.8	1.4	2.0	2.5	1.6	2.2	4.0	4.0	4.0	3.5	4.7	2.4	3.8
P ₁₅	1.7	2.8	2.4	1.6	1.4	2.0	2.4	1.5	2.1	3.3	3.4	4.1	3.0	3.8	2.5	3.4
P ₁₆	1.6	2.5	2.3	1.6	1.4	1.7	2.0	1.5	1.9	2.8	3.2	4.1	2.5	3.8	2.6	3.2
P ₁₇	1.7	2.5	2.5	1.6	1.4	1.8	2.1	1.5	2.1	3.3	3.9	4.6	2.8	3.8	2.4	3.6
P ₁₈	1.6	2.4	2.3	1.6	1.4	1.7	2.0	1.5	1.8	2.7	3.1	3.9	2.3	3.5	2.7	3.1
BMA	1.6	2.4	2.4	1.6	1.4	1.8	2.0	1.5	1.8	2.7	3.1	3.9	2.3	3.6	2.7	3.4

chosen, from roughly 40% in the iid case to 77% for the autoregressive model. Method P₈ saw a more modest increase of 5% in the frequency at which the 0.8 quantile was chosen.

Method P₁₂ is extremely sensitive to rounding, with average differences of around 57% in the proportion of times the 0.8 quantile was chosen as threshold. The reason for this is that the null distribution in the software implementation is obtained by calculating the goodness-of-fit measure based on simulated samples, which are not rounded. Introducing rounding in the parametric Monte Carlo approximation to p -values would solve this. Methods P₉, P₁₄, P₁₅ and P₁₇ are also affected, to a lesser degree, especially for the Weibull distribution (d).

- The modal quantile level for many procedures is 0.8, the lowest candidate. The procedures of [Thompson et al. \(2009\)](#) (P₅), [Northrop and Coleman \(2014\)](#) (P₇) and [Silva Lomba and Fraga Alves \(2020\)](#) (P₁₃) select higher thresholds.
- Application of ForwardStop (not shown) leads to lower thresholds and is thus is not recommended, as most methods generally give low thresholds.
- The methods of [Thompson et al. \(2009\)](#) (P₅), [Süveges and Davison \(2010\)](#) (P₆), [Northrop, Attalides and Jonathan \(2017\)](#) (P₁₁), [Silva Lomba and Fraga Alves \(2020\)](#) (P₁₃) and [Kiran and Srinivas \(2021\)](#) (P₁₄) lead to much less agreement and greater variability of selected quantile levels. For P₁₁, this tallies with Table 2 of [Murphy, Tawn and Varty \(2025\)](#).
- [Wadsworth \(2016\)](#) (P₉) sequential testing fails 33% of the time, even after reducing the number of thresholds considered, jittering data, and with sample sizes of 1000 observations. It performs worst with heavy-tailed distributions, but is generally competitive when it works.
- The procedures of [Caers, Beirlant and Maes \(1999\)](#) (P₂), [Wadsworth \(2016\)](#) (P₉) and [Murphy, Tawn and Varty \(2025\)](#) (P₁₇) perform well relative to the oracle.
- By construction, the [Collings et al. \(2025\)](#) TAILS method (P₁₈) selects higher thresholds than [Murphy, Tawn and Varty \(2025\)](#) (P₁₇) and thus performs better than the latter for heavy-tailed distributions. Both methods outperform [Varty et al. \(2021\)](#) (P₁₆).

- The Bayesian model averaging method of [Northrop, Attalides and Jonathan \(2017\)](#) is competitive in all scenarios. In our simulation, the posterior weights of each quantile levels tended to be more or less uniformly distributed over the set of candidates, with less weight for the largest quantiles.

C.3 Simulation 2

Many of the semiparametric methods are not directly comparable with their likelihood-based counterparts because they choose an order statistic among all possible choices, rather than a threshold from a candidate set. Most such methods (except S_3 and S_{14}) are based on Hill's estimator, and designed for positive shape parameters, a major practical limitation. Moreover, most methods are designed to provide good point estimators of the shape, which are seldom of interest *per se*; there is no guarantee that these properties carry over to risk measures.

We compared the following procedures, most of which are implemented in the **R** packages `tea` ([Ossberger, 2020](#)) and `mev` ([Belzile, 2026](#)):

- S₁. minimization of the asymptotic mean squared error of the Hill estimator ([Hall and Welsh, 1985](#));
- S₂. smoothing and bootstrap estimation of the mean squared error ([Hall, 1990](#));
- S₃. the exponential generalized quantile threshold of [Beirlant, Vynckier and Teugels \(1996b\)](#);
- S₄. the bias-reduction method of [Drees and Kaufmann \(1998\)](#);
- S₅. minimization of the asymptotic mean squared error of the Hill estimator, estimated using a nonparametric double bootstrap ([Danielsson et al., 2001](#));
- S₆. the bootstrap diagnostic test for exponentiality of log-spacings ([Guillou and Hall, 2001](#));
- S₇. the non-robust prediction error C -criterion (non-robust version) of [Dupuis and Victoria-Feser \(2003\)](#);
- S₈. minimization of ([Reiss and Thomas, 2007](#), p. 137)

$$\frac{1}{n_u} \sum_{i=n-n_u}^n i^\beta |H_{n,i} - \text{med}\{H_{n,n}, \dots, H_{n,i+1}\}|^p, \quad 0 \leq \beta < \frac{1}{2},$$

for $p = 1$, with $\beta = 0$ based on recommendations from [Neves and Fraga Alves \(2004\)](#) for Hill's estimator with heavy-tailed data;

- S₉. [Reiss and Thomas \(2007\)](#), as above but with $p = 2$;
- S₁₀. Jackson kernel-based threshold selection ([Goegebeur, Beirlant and de Wet, 2008](#));
- S₁₁. minimum distance threshold selection ([Clauset, Shalizi and Newman, 2009](#));
- S₁₂. minimization of the asymptotic mean squared error of the Hill estimator, estimated using a double nonparametric bootstrap scheme ([Gomes, Figueiredo and Neves, 2012](#));
- S₁₃. a heuristic algorithm based on sample path stability ([Gomes et al., 2013](#));
- S₁₄. the random block maxima estimator of [Wager \(2014\)](#) with empirical risk minimization;
- S₁₅. a variant of [Hall \(1990\)](#) that estimates second-order parameters ([Caeiro and Gomes, 2014](#));
- S₁₆. minimization of the asymptotic mean squared error of the Hill estimator ([Caeiro and Gomes, 2016](#), § 2);
- S₁₇. the eyeballing technique of [Danielsson et al. \(2019\)](#) based on moving windows for the Hill plot;
- S₁₈. minimization of the mean absolute deviation between the largest observations of the dataset and the theoretical generalized Pareto tail ([Danielsson et al., 2019](#)), estimated using Hill's estimator;

- S₁₉. the procedure of Danielsson et al. (2019), but with the Kolmogorov–Smirnov distance;
- S₂₀. minimization of the asymptotic mean squared error based on the relationship between Hill and trimmed Hill estimators of Bladt, Albrecher and Beirlant (2020);
- S₂₁. smooth estimation of the asymptotic mean squared error of the generalized jackknife estimator (SAMSEE) of Schneider, Krajina and Krivobokova (2021).

In each case we return the selected threshold, the number of exceedances, the shape parameter estimate and Weissman’s quantile estimate at level 0.999. All methods but S₃ and S₁₄ use the Hill estimator. The exponential regression model shape estimator can be negative and, although the estimator described in Remark 2 of Beirlant, Dierckx and Guillou (2005) could be used, results would not be easily comparable. As such, quantile are omitted for this method.

Robustness of semiparametric methods

We performed a simulation similar to that of Simulation 1 for rounding and serial correlation, and for determining the effect of sample size on estimates. We focus on generalized Pareto distributions, and those for which the penultimate shape parameter is positive.

Impacts of rounding and truncation The effect of rounding was not particularly noticeable on the quantile level of the thresholds (Figure 12). On the contrary, serial correlation generally leads to the selection of lower quantiles for heavier-tailed distributions. Failing to account for dependence leads to positively biased shape estimators and thus to fairly systematic overestimation of high quantiles for heavy-tailed distributions (Figure 13). Methods S₃ and S₁₄, which use different shape estimators, appear more robust to autocorrelation.

Sample size We consider two different schemes for assessing the impact of sample size and to see whether, in larger samples, increasingly high quantile levels are selected as thresholds.

In the first scheme, we consider samples of size $n = 2000$, and consider the effect of restricting selection to $n = 1000$ top observations (i.e., above the sample median) or allowing all $n = 2000$ as candidate thresholds. Figure 14 shows the distribution of the proportion of exceedances, n_u/n , per method and over all distribution scenarios. It shows quantiles of the density, truncated to the range $[0.1, 0.9]$, for the unconstrained case (all) and the restricted case. Many methods are very sensitive to the non-extreme observations, and for most the range of selected values for n_u becomes both more variable and wider when non-extreme observations are selected as thresholds. Methods S₂, S₃, S₅–S₇, S₁₁–S₁₅ and S₂₁ all see a much wider range for the distribution of n_u/n when unrestricted, though the opposite can occur with light-tailed distributions. Generally, selecting lower thresholds (larger n_u) in these heavy-tailed scenarios leads to a large increase in the shape parameter estimates (Figure 16) which also become much more dispersed, biasing the estimated quantiles (Figure 15) and increasing the variability of the sampling distribution of the parameter estimators.

In the second scheme, we consider samples of sizes $n = 1000, 2000, 3000, 4000$. For most methods and distributions, and as one would hope, the quantile level of the threshold increased with n . Methods S₁₇ and S₁₉ select very high quantiles (higher than the 0.98 quantile), and likewise for S₂₁ for non-heavy tailed distributions. Some methods such as S₂₀ (Bladt, Albrecher and Beirlant, 2020) and the MAD minimization of Danielsson et al. (2019) (S₁₈) had near constant proportions of exceedances, while this was the case only for some distributions for S₅. Figure 17 shows how this proportion generally decreases, even if n_u increases.

Summary of findings for Simulation 2

Figures 10 and 11 suggest the following:

- The Hill estimator struggles with distributions for which ξ is low, but excels for very heavy-tailed distributions. The exponential estimator and the random block maxima are more variable for the latter case.
- Estimates of the 0.999 quantile are more or less adequate even when the Hill estimator is inapplicable, at least if the penultimate behaviour of the distribution is positive.
- The Beirlant, Vynckier and Teugels (1996a) procedure (S_3) is extremely variable, both for the selection of n_u and for the estimation of ξ . It often fails to fit.
- The methods of Hall and Welsh (1985) (S_1) and Caeiro and Gomes (2014) (S_{13}) behave erratically with small shape parameters, giving shape parameter estimates that show strong upward bias. They retain more than 15% of the data for inference, and thus have a tendency to systematically overestimate high quantiles. For method S_{13} , the median of the ratio of 0.999 to the true quantile is about three.
- The proposal of Schneider, Krajina and Krivobokova (2021) (S_{21}) works well in the heavy-tailed case;
- The AMSE minimisation procedures of Caeiro and Gomes (2016) and Gomes, Figueiredo and Neves (2012) display low relative root mean squared error for quantile estimation, consistently across all scenarios, but can fail catastrophically for particular datasets.
- The method with the lowest relative bias for quantiles is Guillou and Hall (2001), and the lowest mean square errors are obtained using the Danielsson et al. (2019) minimization of the Kolmogorov–Smirnov distance (for $\xi < 0.25$) and Bladt, Albrecher and Beirlant (2020) ($\xi \geq 0.5$);
- The Drees and Kaufmann (1998) procedure fails to return valid values for n_u in around 80% of cases. When it works, it leads to small values of n_u , and to shape estimates that are below average; the width of the confidence intervals in Figure 10 suggests excess variability. We have not fixed the tuning parameter of the stopping criterion to unity throughout.
- The Dupuis and Victoria-Feser (2003) estimator leads to very small n_u , and thus variable and negatively-biased shape estimates, but performs best for quantile estimation for low shape parameter.
- The sampling distributions of the shape parameters for the methods of Reiss and Thomas (2007) (S_8 and S_9) are left-skewed.
- The procedure of Wager (2014) (S_{14}) provides only an estimate of the shape parameter, and performs very poorly when coupled with Weissman’s estimator, with systematic underestimation of return levels; more work is needed to derive a suitable estimator of the quantile.

The more computationally-intensive methods use the bootstrap. The double bootstrap takes over two minutes to run with 1000 exceedances.

Appendix D: Applications to data

We considered threshold selection methods for four datasets commonly used in the literature for comparison purposes. These are

1. the River Nidd levels in Yorkshire [$n = 154$, `nidd.thresh`, `evir` package],
2. the Danish fire loss [$n = 2167$, `danish`, `evir` package],

3. the Fort Collins precipitation series [$n = 4147$, `FCwx`, `extRemes` package]
4. the North Sea wave height hindcast data [$n = 628$, `ns`, `threshr` package].

For the Fort Collins data, we consider only rainfall between April and November to avoid glaring nonstationarity.

The results are shown in Table 6. The first three datasets exhibit heavy tails, while the wave height dataset clearly has a bounded upper tail. Many algorithms for semiparametric methods select very low thresholds for which there are a larger number of exceedances; only providing the largest 1000 or 500 observations, say, would yield different thresholds, as reported in Simulation 2. The [Wadsworth \(2016\)](#) method fails on the first two datasets, but can be fixed by selecting just a handful of thresholds. For the Nidd data, the parametric methods select either the highest threshold or nearly all observations.

Appendix E: Omitted methods

Although some may have escaped our scrutiny or have appeared very recently, we have attempted to describe and compare most threshold selection methods in the literature. Others sketched below were excluded from the simulations for a variety of reasons.

E.1 Mean residual life plot

[Mínguez \(2025\)](#) includes additional tests, routinely used in linear regression, for outliers based on internally studentized residuals (for the smallest observation) and goodness-of-fit assessment based on the variance of these residuals. He also suggests fitting smoothing splines to the mean squared error values to identify local minima, but the spline ignores the serial correlation of these values and differences in variance of the point estimates. The multi-stage procedure seems to us overly complex.

E.2 Parameter stability plots

[Curceac et al. \(2020\)](#) propose to fit a penalized cubic spline to smooth parameter estimates in parameter stability plots until a plateau emerges. The detection of the latter is difficult, and the method does not account for the dependence of successive estimators.

E.3 Robust methods

Robust estimation methods can downweight observations that do not conform with the model, thereby reducing their influence on the fit, but comes at the expense of a loss of information (cf. [Davison and Smith, 1990](#), §5). [Dupuis \(1999\)](#) proposes an optimal B -robust estimator of the generalized Pareto parameters, which returns both parameter estimates and weights for observations. In the upper tail, the weights are non-increasing as the quantile increases. Poorly-fitted points are downweighted and thus suspected not to be drawn from the limiting model, but observations from the GPD itself might also be downweighted, so simulation is needed to calibrate the weights. To avoid multiple testing, we used a cusum statistic based on the m non-zero weight of the upper tail fit to the original data, and approximated the null distribution by computing the weights for samples drawn from a GPD using the optimal bias-robust estimator. We get strong indication of missfit for thresholds lower than the 98% for the Padova data, leading to $u = 42.77\text{mm}$. The repeated fit is too computationally expensive to consider in a simulation study, and more work on calibration and the choice of summary statistic would be needed for this approach to be properly automated.

Table 6 Number of exceedances at chosen threshold for four standard datasets. For parametric methods (bottom), candidate thresholds consisted of 21st, 31st, . . . , 151st order statistics (Nidd river data), empirical quantiles at level 0.8, 0.81, . . . , 0.99 (Fort Collins precipitation and Danish insurance data), and empirical quantiles at level 0.5, 0.55, . . . , 0.90 quantiles (North Sea wave height). Methods with em-dash (—) indicate that no threshold is returned. Stars (*) indicate a procedure run with different or smaller number of thresholds.

method	Nidd	Danish	Fort Collins	North Sea
Hall and Welsh (1985)	153	19	387	
Hall (1990)	141	81	150	
Beirlant, Vynckier and Teugels (1996a)		770		
Drees and Kaufmann (1998)		64		
Danielsson et al. (2001)	139	1262	10	
Guillou and Hall (2001)	102	84	61	
Dupuis and Victoria-Feser (2003) (non-robust)	21	26	10	
Reiss and Thomas (2007) (l_1)	147	1661	66	
Reiss and Thomas (2007) (l_2)	137	1547	43	
Goegebeur, Beirlant and de Wet (2008)	145	1796	699	
Clauset, Shalizi and Newman (2009)	89	1564	586	
Gomes, Figueiredo and Neves (2012)	91	1285	13	
Gomes et al. (2013) (sample paths)	140	1551	419	
Wager (2014)	77	94	2073	
Caeiro and Gomes (2014)	86	1163	11	
Caeiro and Gomes (2016) (AMSE)	67	546	33	
Danielsson et al. (2019) (eye-balling)	6	21	50	
Danielsson et al. (2019) (MAD)	12	17	206	
Danielsson et al. (2019) (KS)	16	95	6	
Bladt, Albrecher and Beirlant (2020)	54	591	318	
Schneider, Krajina and Krivobokova (2021) (SAMSEE)	77	944	59	
Pickands (1975)	89	174	362	157
Davison and Smith (1990)	20	260	810	283
Caers, Beirlant and Maes (1999)	149	434	737	314
Thompson et al. (2009)	20	174	162	314
Northrop and Coleman (2014)	40	65	125	95
Langousis et al. (2016)	149	434	810	157
del Castillo and Padilla (2016)	39	174	810	314
Wadsworth (2016)			810	157
Northrop, Attalides and Jonathan (2017)	127	434	810	189
Bader, Yan and Zhang (2018)	149	195	39	189
Silva Lomba and Fraga Alves (2020)	20	22	39	220
Varty et al. (2021)	149	434	810	314
Kiran and Srinivas (2021)	133	195	125	157
Gamet and Jalbert (2022) (beta EGP model)		195	572	189
Murphy, Tawn and Varty (2025)	30	195		314

E.4 Coefficient of variation stability

del Castillo and Padilla (2016) propose using the coefficient of variation for diagnostics and formulate an automated procedure for exceedances of a fixed grid \mathcal{U} of thresholds. A generalized Pareto random variable $GP(\sigma, \xi)$ has coefficient of variation $cv(X) = sd(X)/E(X) = (1 - 2\xi)^{-1/2}$, which does not depend on the scale parameter and yields a consistent moment-based shape estimator if $\xi < 1/2$, which, if $\xi < 1/4$ and suitably renormalized, converges in distribution to a Gaussian process with constant mean and known covariance function. Standard results can be then be used to test whether a realisation of this process has a constant mean. del Castillo and Padilla (2016) suggest parametric bootstrap approximations of

the distribution of a related statistic, leading to a sequential procedure that starts with the smallest threshold and stops when the bootstrap p -value is lower than a level α . They also propose transformations that deal with the effect of the constraint $\xi < 1/4$, which limits the applicability of the idea for heavy-tailed data. However, the transformation affects the rate of convergence of the penultimate approximation (Wadsworth, Tawn and Jonathan, 2010): one needs estimates of σ and ξ , which depend on the threshold, and their methodology requires a preliminary test of the moment condition. Simulation results indicated that this approach is amongst the worst we considered, leading to systematic selection of the lowest possible threshold whenever applicable. We have opted not to discuss it further. It also fails often, and cannot be recommended.

E.5 Smoothing of Hill's estimator

Schneider, Krajina and Krivobokova (2021) use related ideas for the inverse Hill statistic, which approximates the mean integrated squared error of Hill's estimator relative to an exponential density. They use Bayesian nonparametric methods to smooth the resulting estimates and pick n_u for which the smoothed mean is smallest. The empirical Bayes procedure proposed for the smoothing is computationally intensive in medium to large samples, and the degree of smoothing was unsatisfactory in our numerical work.

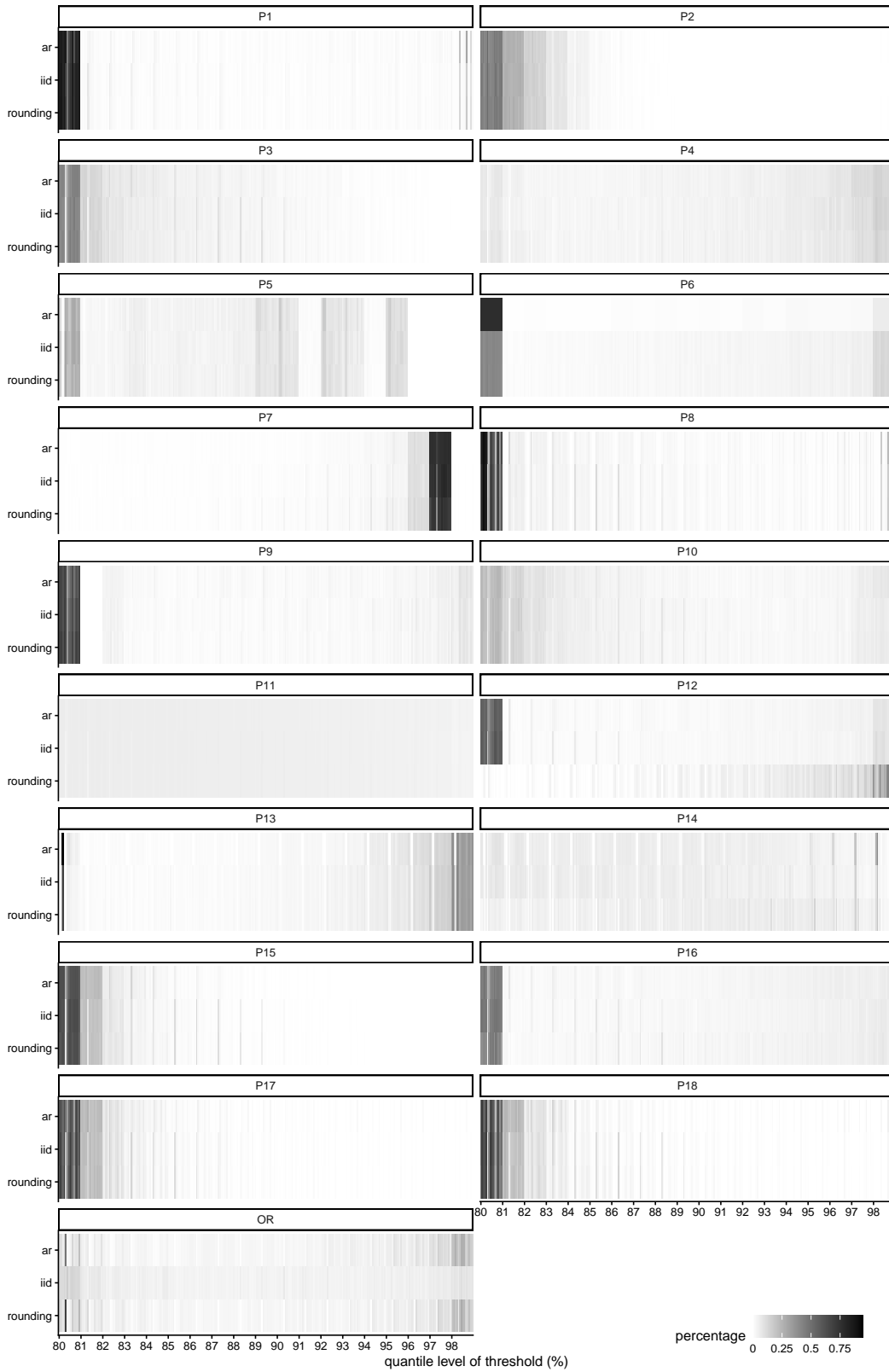


Figure 8 Heatmap of the percentage of threshold selection per method for each of the different quantile levels (*x*-axis, from left to right), across scenarios (*y*-axis) and distributions a–p (panels).

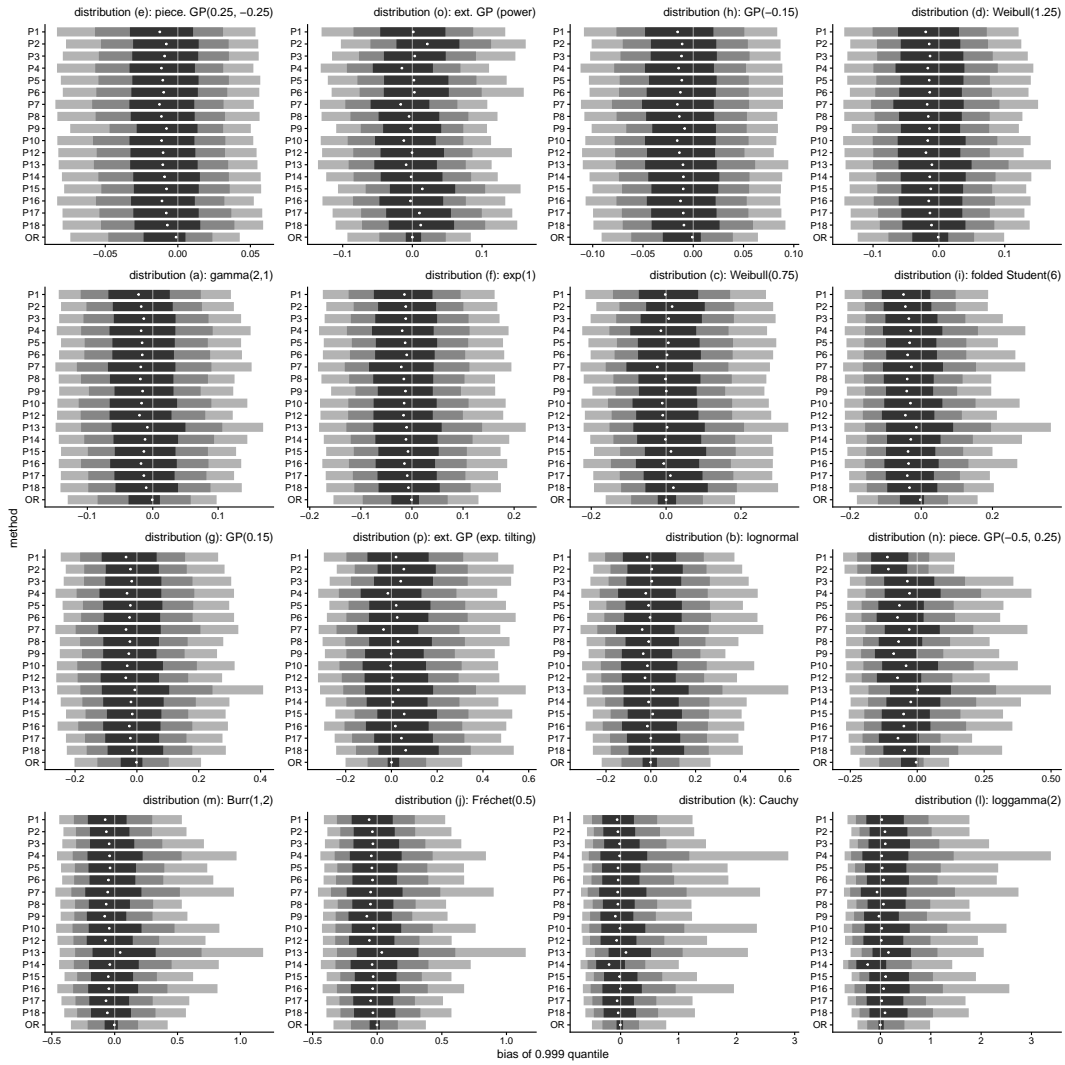


Figure 9 Results of Simulation 1: median (white circles), 50% (dark grey), 80% (grey) and 95% (light grey) bands for the relative bias of the 0.999 quantile, based on maximum likelihood estimates using candidate thresholds at the 0.8, 0.81, ..., 0.98 sample quantiles taken from $n = 2000$ independent and identically distributed observations. The distributions are ordered in increasing level of the penultimate shape parameter (vertical black line) at level 0.999.

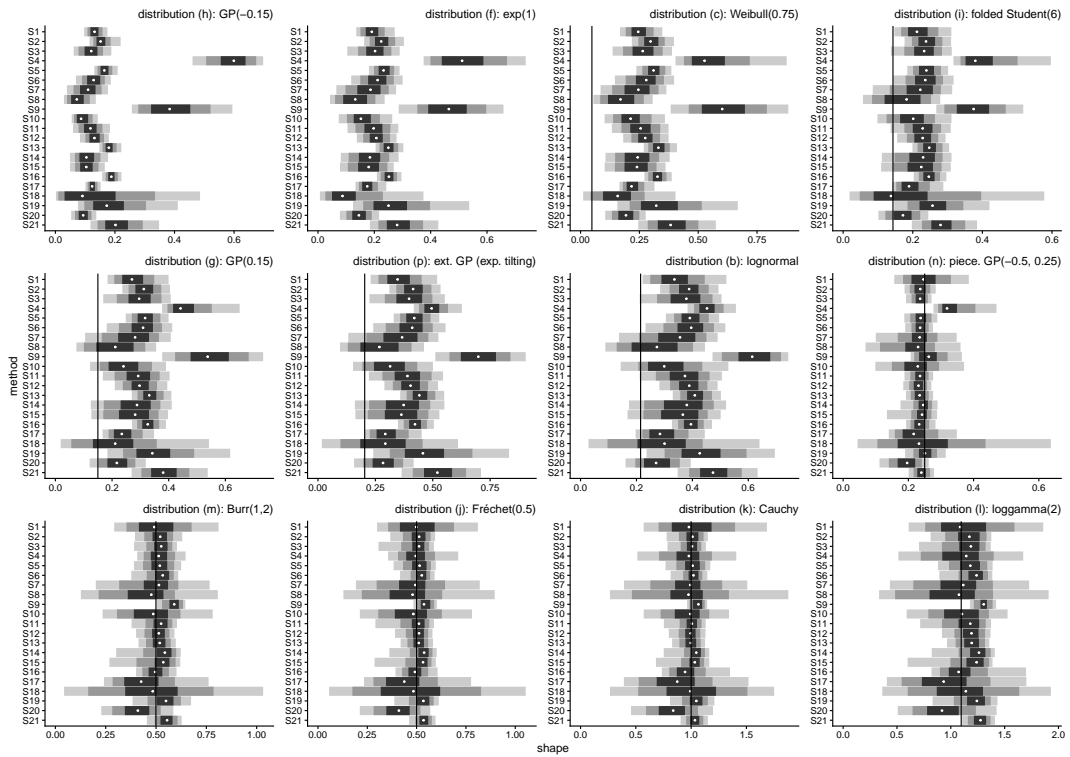


Figure 10 Results of Simulation 2: density plots with median, 66% and 95% bands for the shape parameter estimates (top), as a function of the distribution, method for samples of $n = 2000$ independent and identically distributed observations. The distributions are ordered by increasing level of the penultimate shape parameter (vertical black line).

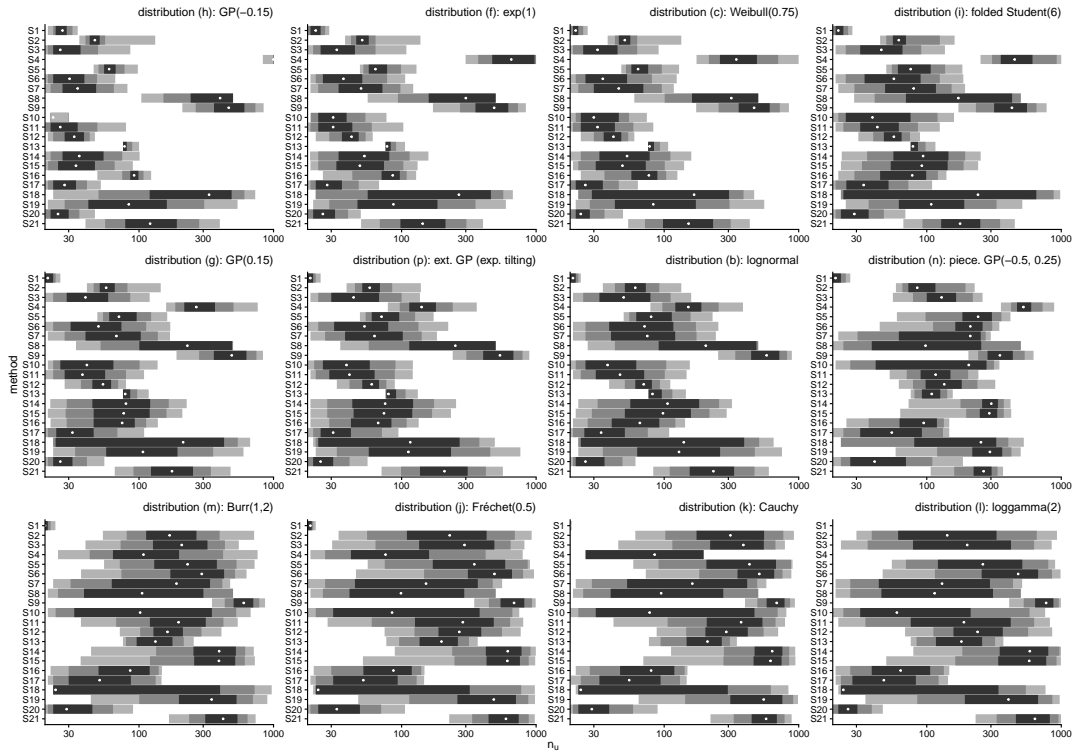


Figure 11 Results for Simulation 2: median (white point) 50% (dark grey), 80% (grey) and 95% (light grey) confidence bands for the rank of the threshold (with the number of exceedances on the x-axis shown on the log-scale), chosen as the $(n - n_u)$ th order statistic with the same settings of Figure 10.

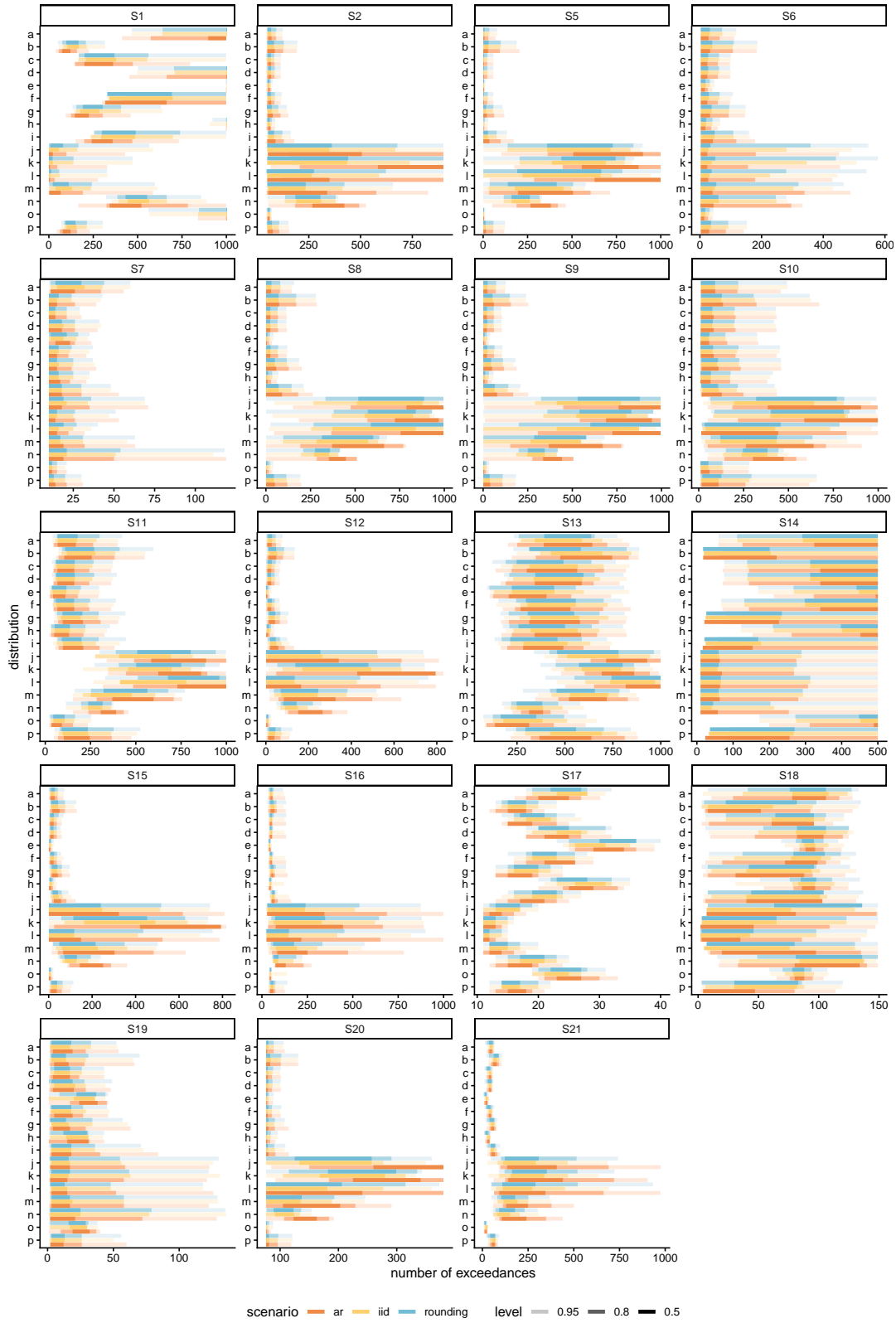


Figure 12 Results for Simulation 2: 50%, 80% and 95% (shade) highest density continuous intervals for the number of exceedances for different scenarios (independent and identically distributed, serially correlated and rounded).

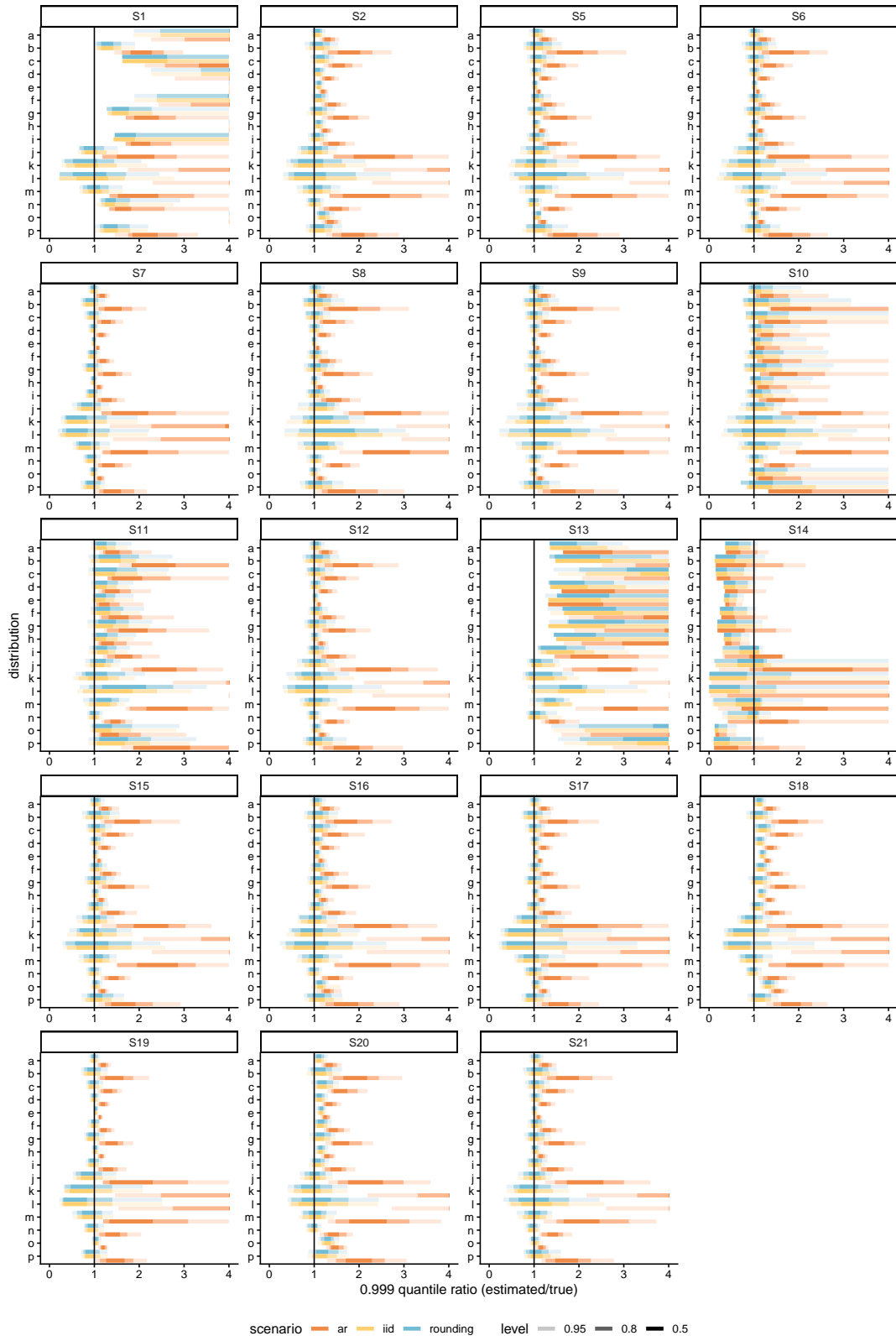


Figure 13 Results for Simulation 2: 50%, 80% and 95% highest density continuous intervals for the ratio of the 0.999 quantile estimate, relative to the true theoretical counterpart.

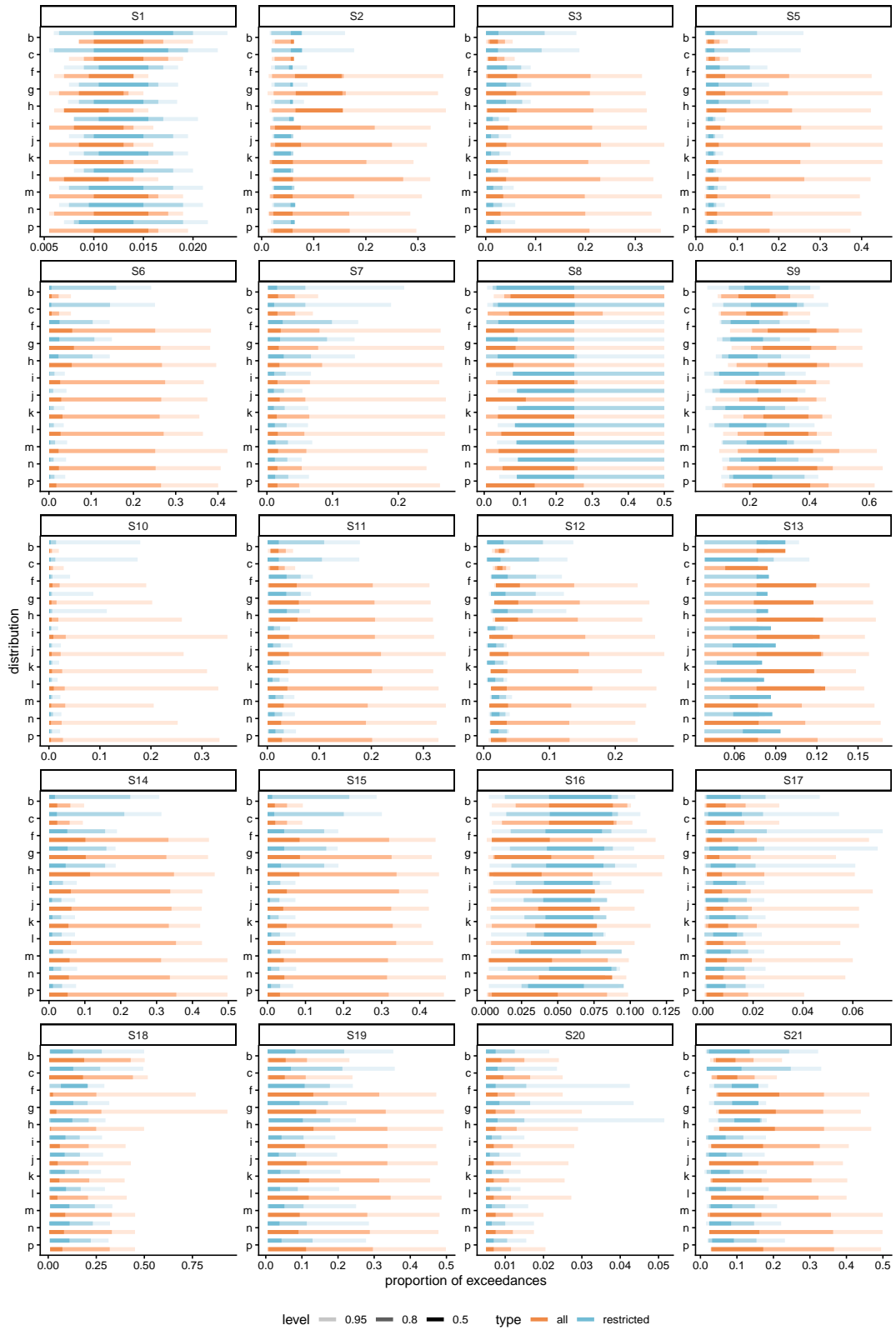


Figure 14 Results for Simulation 2: 50%, 80% and 95% highest density continuous intervals for the proportion of exceedances relative to the sample size for $n = 2000$, when restricting the largest 50% or not (color).

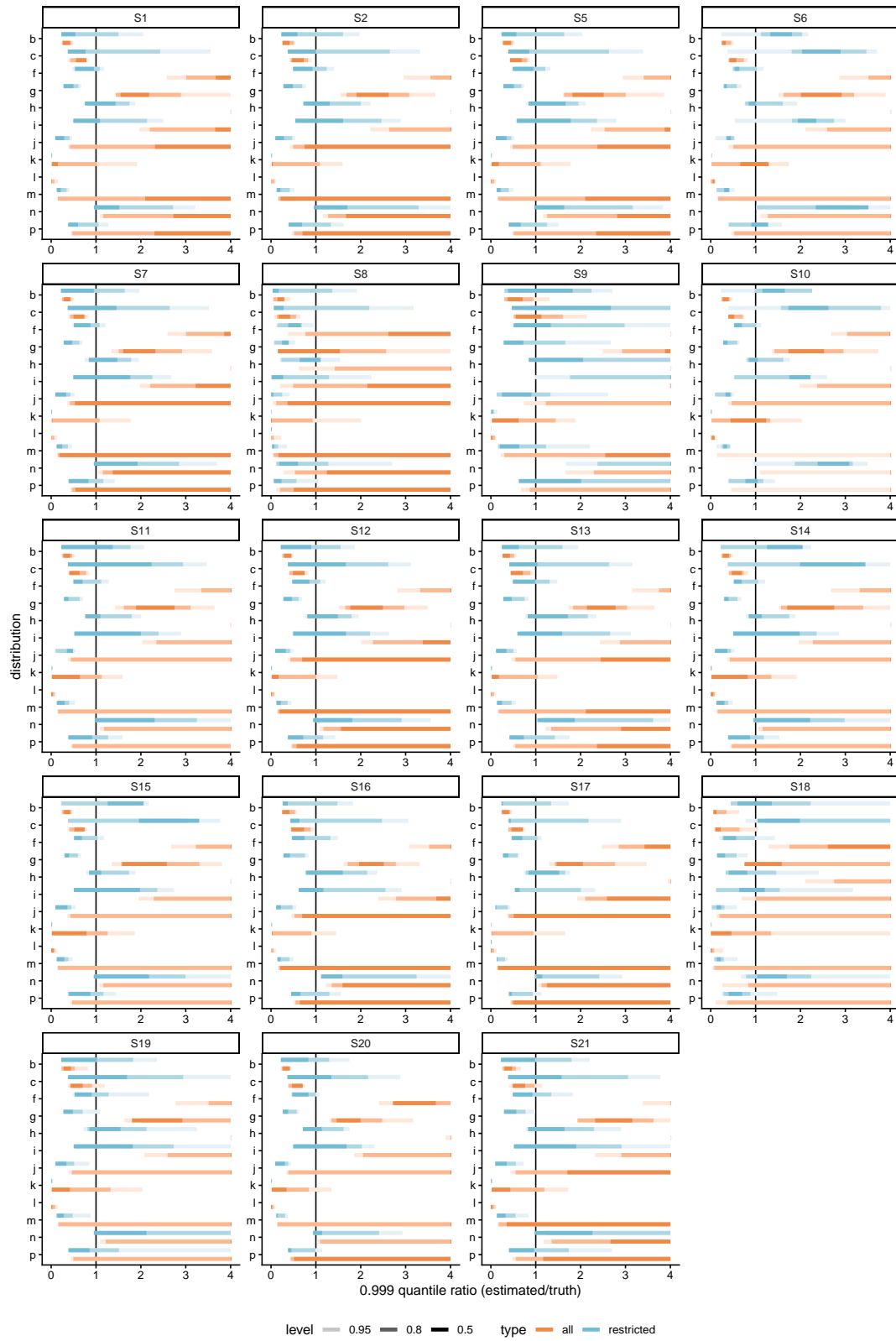


Figure 15 Results for Simulation 2: 50%, 80% and 95% highest density continuous intervals for the ratio of estimated 0.999 quantile to the true theoretical counterpart, when restricting the largest 50% or not (color). The ratio is capped at 4 in the plot.

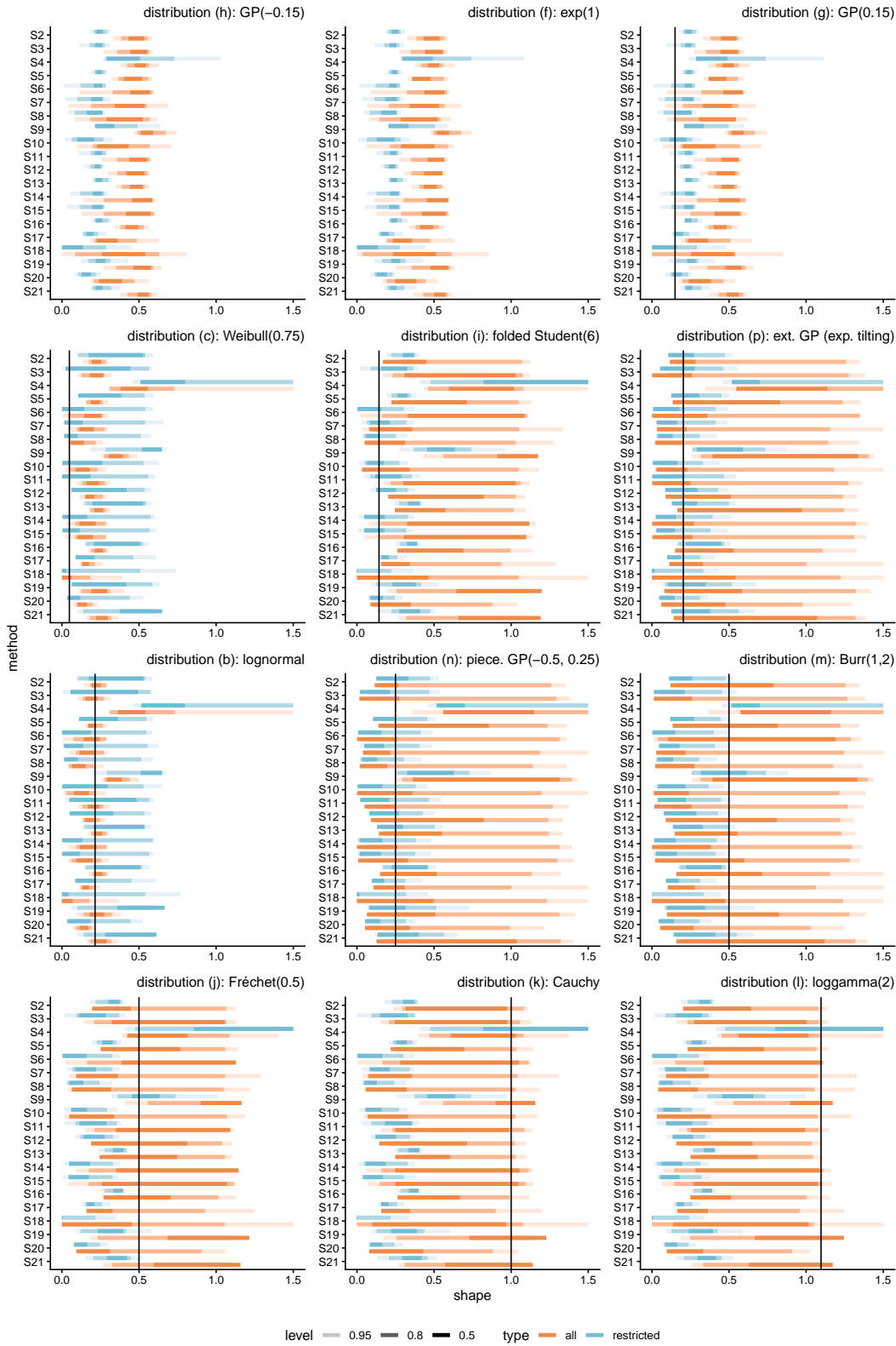


Figure 16 Results for Simulation 2: 50%, 80% and 95% highest density continuous intervals for the shape parameter estimates for generalized Pareto models (top row) and models with penultimate approximations and heavy tails. The vertical bar in each panel gives the value of the penultimate shape parameter at the 0.999 quantile.

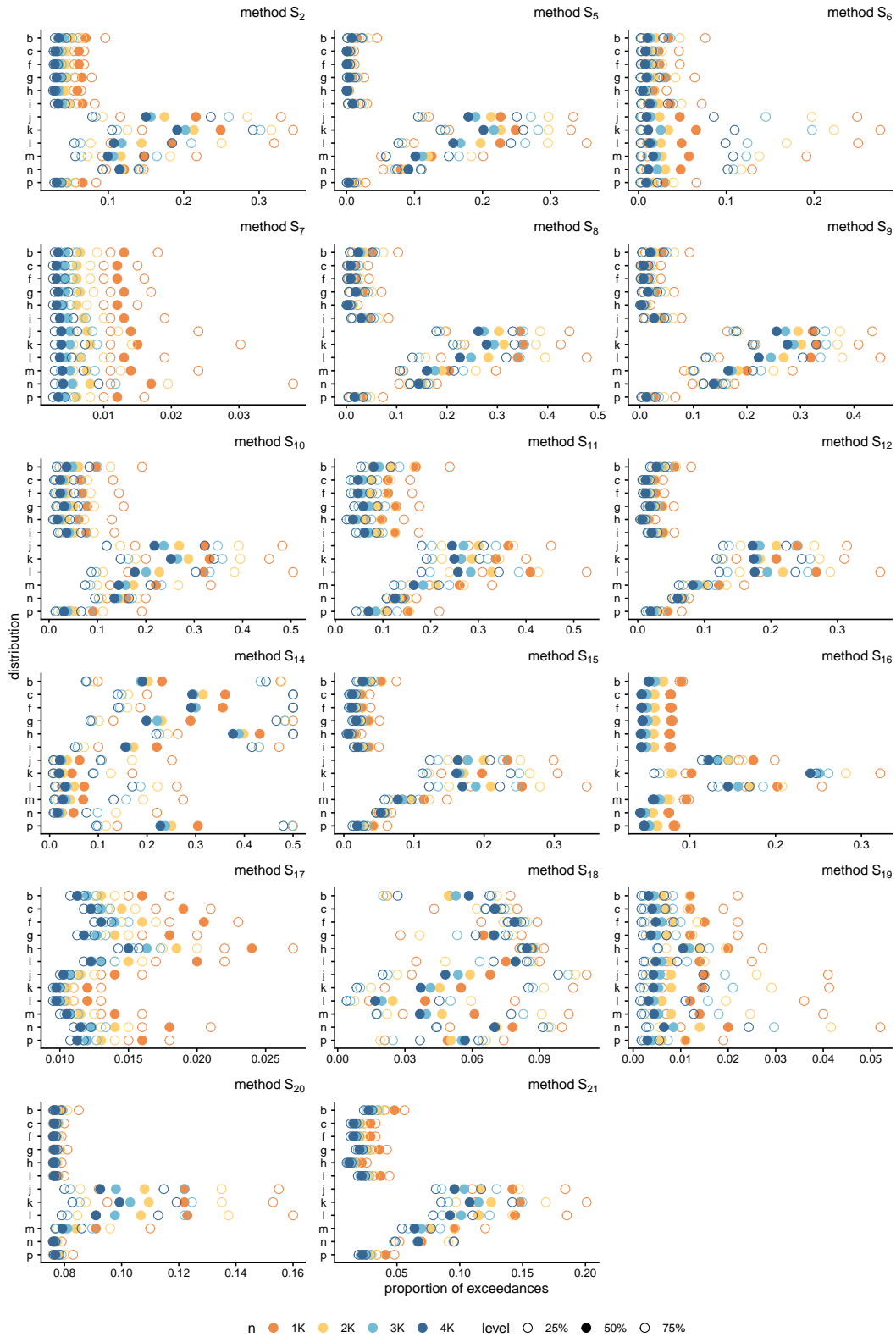


Figure 17 Results for Simulation 2: quartiles and median (full circle) of the percentage of exceedances relative to the total sample size $n \in \{1000, 2000, 3000, 4000\}$ (x-axis) for each distribution (y-axis) and for selected threshold selection methods (panel), as a function of the sample size (color).